



Experimental study on a two-dimensional ultrasonic vibration platform and milling of Ti₂AlNb intermetallic alloy

Zhaojie Yuan¹ · Guofu Gao¹ · Yi Wang¹ · Zongxia Fu¹ · Daohui Xiang¹

Received: 30 November 2021 / Accepted: 25 June 2022 / Published online: 4 July 2022
© The Author(s), under exclusive licence to Springer-Verlag London Ltd., part of Springer Nature 2022

Abstract

In order to solve the problems of poor machining accuracy and surface quality of hard and brittle materials such as Ti₂AlNb intermetallic alloy in conventional machining, the principle of apparent elasticity method was used to design a flat-plate vibration device. Firstly, the propagation characteristics of ultrasonic in inclined slot plate were analyzed by using the propagation law of acoustic wave in different media. Secondly, the vibration characteristics were analyzed and discussed in detail by using finite element software. Finally, the influence of the vibration characteristics of vibration platform on the cutting performance of Ti₂AlNb alloy was studied through ultrasonic vibration cutting and common cutting (CC) experiments. The finite element modelling (FEM) and test results showed that when the slot width was 2 mm and the inclination angle was 45°, the vibration effect of the plate vibration device was the best, and the vertical upward vibration component was generated at the workpiece installation area of the plate. The errors between the measured frequency and the results of theoretical calculation and finite element analysis were 1.78% and 0.36%, respectively, which showed the reliability of finite element simulation. Compared with the three-dimensional ultrasonic vibration cutting (3DUVC) and CC, the results of two-dimensional ultrasonic vibration cutting (2DUVC) based on flat-plate vibration device showed an obvious “drainage tank” microstructure in variable speed cutting; when the rotating speed was 1700 r/min, the roughness value of 2DUVC was 54% and 57% lower than that of 3DUVC and CC, respectively. The amplitude along the feed direction was 8 μm, the surface roughness of 2DUVC decreased by 64% and 65.9%, respectively, compared with 3DUVC and CC. The number of chip sawtooth increased with the increase of ultrasonic amplitude and vibration dimension. The experimental results showed that for Ti₂AlNb alloy, ultrasonic vibration cutting can obtain higher surface quality, and the two-dimensional ultrasonic vibration platform was helpful to improve the cutting performance of materials, and the 3DUVC can realize the rapid removal of materials.

Keywords Vibration platform · Simulation analysis · Vibration characteristics · Amplitude · Ti₂AlNb intermetallic alloy · Surface topography · Sawtooth chip

1 Introduction

Ti₂AlNb alloys, based on their higher specific strength, heat resistance, and corrosion resistance than nickel-based alloys, super-alloys, and titanium alloys, are widely used in high-precision fields such as aviation, aerospace, and modern national defense [1]. However, the problem of poor machining performance coexists with the excellent service performance of this kind of materials. When the common cutting (CC) process is used for precision machining of this

kind of materials, the disadvantages of high brittleness, easy to stick to the tool, and high cutting temperature in the precision machining of this kind of materials lead to the adverse consequences of tool damage and poor machining quality, resulting in the CC process cannot get the ideal machining effect [2–4]. In recent years, the rapid development of ultrasonic vibration cutting technology shows unique advantages in the precision machining of hard and brittle materials, especially in reducing cutting force, cutting heat, and improving surface quality [5–8], which is widely used in the machining of hard, brittle, and difficult-to-machine materials.

With the rapid development of technology in the high-tech field, the requirements of parts for machining quality are also increasing. The vibration mode of ultrasonic

✉ Guofu Gao
gaogf@hpu.edu.cn

¹ School of Mechanical and Power Engineering, Henan Polytechnic University, Jiaozuo 454000, Henan, China

unidirectional vibration cannot meet the requirements of actual machining. Therefore, ultrasonic multi-dimensional composite vibration has become a research hotspot. At present, the widely used ultrasonic composite vibration modes mainly include longitudinal bending composite vibration [9], longitudinal torsional composite vibration [10, 11], double bending composite vibration [12] and elliptical ultrasonic vibration [13], which have achieved good machining results. However, these ultrasonic vibration machining processes impose vibration on the tool, which limit the application scope of ultrasonic machining to a certain extent and cannot meet the needs of complex and changeable actual machining. Therefore, the ultrasonic vibration form of workpiece becomes particularly important. Because the volume of the workpiece is generally large, if it is directly used as a load at the transmitting end of the ultrasonic vibration device, the ultrasonic vibration effect will be greatly reduced. Until now, there is less research in this field, but the high-frequency vibration applied to the workpiece can cause fatigue damage to the workpiece material, promote the grain slip in the material, and then change the micro-mechanical properties of the material, resulting in a reduction in the yield point, strength, and plastic deformation resistance of the material, which are conducive to improving the efficiency of cutting [14, 15]. Meanwhile, the workpiece vibration is more convenient for the application of vibration of the acoustic system, and the coupling processing of multi-dimensional vibration system can be realized.

According to the different application positions of ultrasonic vibration, the ultrasonic vibration of workpiece can be divided into two vibration forms. One is that the vibration is directly applied to the workpiece, and the other is that the vibration is indirectly applied to the workpiece; that is, the vibration is applied to the workbench fixing the workpiece. The second form is less affected by the workpiece shape and the workspace of the workpiece in practical application. The most common form of vibrating workbench is rectangular plate. Many scholars used different methods to study its vibration characteristics. Li and Cheng [16] studied the nonlinear vibration characteristics of rectangular plate by using calculus method and found that when the length width ratio of rectangular plate was equal to 1, the ultrasonic amplitude was positively proportional to the frequency. Qu et al. [17] deduced the general formula for steady-state and transient vibration analysis of shell under arbitrary boundary conditions and verified the effectiveness and accuracy of the formula by comparing it with finite element simulation analysis. Wang et al. [18] proposed a unified solution program based on the first-order shear deformation theory to solve the free vibration analysis of orthotropic medium and thick plates. Li [19] studied the free vibration of rectangular plates with general elastic constraints by using the Rayleigh–Ritz method. The convergence and accuracy of the method were

proved by numerical examples. Li et al. [20] used the energy method to study the lateral vibration characteristics of stiffened rectangular plates under typical boundary conditions and performed numerical calculation analysis. The results showed that the calculation accuracy of this method was better than the finite element analysis, and the convergence was better. Du et al. [21] studied the vibration characteristics of stiffened plates fixed on four sides by using Rayleigh–Ritz method, and the comparison between the calculated results and the experimental values showed good consistency. Paula et al. [22] studied the vibration form of welding thin plate by combining simulation and test. Selicani et al. [23] designed a vibrating plate with genetic algorithm and studied the characteristics of airborne radio wave propagation in the plate using linear acoustic theory. Wang et al. [24] substituted the strain energy and kinetic energy of the plate into the Lagrange equation for solution and studied the solution method and vibration characteristics of the nonlinear vibration of simply supported stiffened plates on four sides. Podymova and Karabutov [25] obtained the frequency correlation of longitudinal and shear ultrasonic attenuation coefficients through ultrasonic nondestructive testing of stainless steel, cast Babbitt alloy, and brass.

The realization mode and vibration effect of two-dimensional ultrasonic vibration have become the focus of researchers, although the one-dimensional longitudinal vibration device has high-power acoustic emission, simple structure, and high mechanical strength and is widely used in power ultrasound and underwater sonar detection applications [26–28]. However, the traditional one-dimensional longitudinal device has a single vibration form, which will limit the direction of ultrasonic radiation in practical application. Researchers have taken some measures to improve the processing effect of one-dimensional longitudinal vibration [29, 30]. For example, the longitudinal torsional vibration produced by the combination of longitudinal and transverse waves can achieve better processing quality than that of one-dimensional longitudinal vibration in cutting and welding. Yin et al. [31] set up a slot on the horn to obtain the output of longitudinal torsional composite vibration through a single longitudinal vibration. Through experimental research, it was found that the inclination, width, and depth of the slot will affect the size of reflected shear wave. Pi [32] based on the reflection principle of the inclined slot on the stress wave, the longitudinal vibration transducer of the unidirectional mode was realized by using the ring inclined slot vibration rod to realize the output of the ultrasonic longitudinal torsional resonance mode. Although the longitudinal torsional composite vibration with single excitation can be obtained by setting a slot, the current research mainly focuses on the horn, and few studies apply it to the rectangular plate. In practical application, rectangular plate is generally heavy as a load, and the amplitude obtained on the radiation surface

after ultrasonic vibration is small, which limits its application to a certain extent.

Some improvement measures have been proposed by researchers in order to obtain a uniformly distributed large amplitude on the radiation surface of the vibrating body. Lin and Zhang [33] found through experimental research that slotting at the vibration node of the rectangular vibrating body can suppress the transverse vibration, and the vibration effect was closely related to the length and width of the slot. Lu and Lu [34] improved the amplitude of the working surface of the vibrating body by opening small slots on the vibrating body. The experiment found that the amplitude of the vibrating body was proportional to the number of slots. Lu et al. [35] arranged two masses symmetrically on the basis of the original Langevin-type transducer to form a transducer with a new structure. Compared with conventional Langevin transducers, it had greater vibration speed, lower temperature rise, and higher electroacoustic energy efficiency. Gao and Lin [36] applied the apparent elasticity method to theoretically analyze the three-dimensional coupled vibration of a large-size rectangular cross-section oblique wedge-shaped horn. The results showed that when the cross-section was relatively small, the one-dimensional theory was closer to the simulation value, while when the cross-section was larger, the three-dimensional theory considering the coupling effect was closer to the simulation analysis result. Xu et al. [37] developed a new two-dimensional dual-mode composite ultrasonic vibration device excited by a single piezoelectric ceramic stack, and conducted experimental research, and found that the vibration device can generate two different resonance modes, which can be applied to new ultrasonic processing technology such as phacoemulsification, ultrasonic defoaming, and ultrasonic sonochemistry. Azarhoushang and Tawakoli [38] invented an ultrasonic vibration system with multi-resonance behavior for rectangular plates, which can apply vibration to heavy parts of various specifications, and conducted ultrasonic vibration grinding experimental research on the workpiece. They found that compared with the traditional grinding process. Compared with, it can reduce about 20% of the grinding force and 30% of the surface roughness.

It can be seen from the above research that the appropriate slot can change the propagation direction of the wave and realize the effect of single excitation and multi-directional vibration. The improved rectangular plate can obtain large amplitude, meet the second form of ultrasonic vibration of the workpiece, and expand the application range of ultrasonic vibration machining.

In order to realize the multi-dimensional ultrasonic vibration machining of hard and brittle materials, based on the existing research on the vibration characteristics of rectangular plates, a plate vibration device was designed based on the principle of apparent elasticity method. The ultrasonic vibration was applied directly to the side of the platform; the refraction and

reflection phenomena of sound wave propagating in different media were applied. Slots were set on the vibration device to change the angle and width of the slot, and the finite element software was used to analyze the vibration characteristics of flat plates with different slot angles and widths. The designed ultrasonic vibration platform was used as the transition device between workpiece and machine tool, the multi-dimensional ultrasonic vibration formed by coupling the longitudinal vibration of the tool with the two-dimensional vibration of the vibration platform; it can be used in ultrasonic vibration cutting process of difficult-to-machine materials. Finally, Ti2AlNb alloy, which is currently difficult to machine in aerospace, was selected as the workpiece material, and the multi-dimensional ultrasonic vibration cutting test was designed, and the vibration characteristics of the vibration platform were inversely verified by analyzing the machined surface quality and chip shape.

2 Theoretical analysis of plate vibration device

2.1 Theoretical design

It is difficult to obtain the analytical solution of the coupled vibration of elastic bodies by using the three-dimensional theory. Based on this, the Japanese scholar Mori Rongsi proposed the apparent elasticity method [39]. Under the condition of considering only the expansion deformation but not the shear deformation, the vibration of homogeneous elastomer is equivalent to the coupling of vertical longitudinal vibration, and the vibration in different directions corresponds to different apparent elastic constants. Therefore, the coupled vibration of the elastomer can be represented by one-dimensional longitudinal vibration in multiple directions, and the vibration of the elastomer is the result of equivalent longitudinal vibration coupling in multiple directions.

The coupled vibration is decomposed into three mutually perpendicular longitudinal vibrations by the apparent elasticity method. The elastic modulus is equivalent to three mutually perpendicular elastic moduli E_x , E_y , and E_z through the Poisson coefficient ν and the coupling coefficients n_1 , n_2 , and n_3 . The frequency equation of any point in the vibrating hexahedron of a rectangular section in all directions was given in [40].

$$\begin{cases} 1 - \frac{\nu(n_1 n_3 + 1)}{n_1} = \frac{\rho^2 A}{E^2} \\ 1 - \frac{\nu(n_1 n_2 + 1)}{n_2} = \frac{\rho^2 A}{E^2} \\ 1 - \frac{\nu(n_2 n_3 + 1)}{n_3} = \frac{\rho^2 A}{E^2} \end{cases} \quad (1)$$

where $A = (C\pi/\omega)^2$, $C = (E/\rho)^{1/2}$, C (m/s) is the speed of sound in a one-dimensional thin rod of ultrasonic wave, E (GPa) is the elastic modulus of the material, n_1 , n_2 , n_3 is the coupling coefficient, and $n_1 n_2 n_3 = 1$.

According to the research in reference [34], the overall frequency equation of three-dimensional coupled vibration of rectangular thick plate can be expressed as:

$$\frac{i^2 j^2 m^2}{l_x^2 l_y^2 l_z^2} A^3 - \left(\frac{i^2 j^2}{l_x^2 l_y^2} + \frac{j^2 m^2}{l_y^2 l_z^2} + \frac{i^2 m^2}{l_x^2 l_z^2} \right) A^2 + (1 - \nu^2) \left(\frac{i^2}{l_x^2} + \frac{j^2}{l_y^2} + \frac{m^2}{l_z^2} \right) A + 2\nu^3 + 3\nu^2 - 1 = 0 \tag{2}$$

when $i=j=m=1$; Eq. (2) is the fundamental frequency equation of rectangular thick plate. The research in literature [33] shows that when the thickness l_z of rectangular plate is less than $(1/4)\lambda$, the thickness direction has little effect on the overall resonant frequency of rectangular thick plate. Considering the requirements of installation, fixation, and workpiece clamping of rectangular vibrating plate, when the plate thickness l_z is 20 mm and $l_x=l_y$, $n_1=1$, and $n_2=1/n_3$, the resonant fundamental frequency of coupled vibration is equal in x and y directions [41], i.e., $f_x=f_y$. The rectangular vibrating plate is made of 45# steel. According to the calculation of combined Formulas (1) and (2), $l_x=l_y=186$ mm.

2.2 The motion of sound waves in a vibrating platform

In the elastic media, vibration energy can be transmitted by sound waves. According to the stress wave theory, all particles in the elastic solid medium are closely related to each other, and the vibration energy of any particle can be transmitted to the surrounding particles, resulting in the vibration of the surrounding particles. The reflection, transmission, and scattering will occur in two media with different densities. In fact, the reflected wave does not have half wave loss, but the result of resisting the vibration source vector. The greater the density difference of the interface medium, the greater the reflection while the smaller the refraction of the wave. Therefore, after the inclined slot and threaded hole are set at the position shown in Fig. 1 of

the flat-plate vibration device, the propagation path of the sound wave will also change due to the existence of the slot. The propagation principle diagram of the sound wave at the position of

the flat-plate inclined slot and threaded hole is shown in Fig. 2.

The vibrating plate is divided into two media with extremely different properties, metal and air, by the slot and threaded holes. The sound wave follows its propagation law in different media. When the slot width or hole is much smaller than the wavelength of the ultrasonic wave, a series of transmission, reflection, and scattering will occur when the wave is transmitted to the slotted position. Since the characteristic impedance of steel is about 5000 times that of air, the air can be assumed to be a vacuum during the propagation of the stress wave in the steel-air medium. At this time, there is only total reflection and no transmission. When the propagation of sound wave P_r in the solid structure encounters the boundary of the plate slot hole, as shown in Fig. 2, the reflected longitudinal wave P_{fz} and reflected transverse wave P_{fh} are generated in the material. The normal strain caused by transverse wave is zero, which will not cause the change of material density, but the shear strain caused by transverse wave is not zero, so the shear force of transverse wave exists. Because the gas and liquid cannot bear the shear force, the effect of the transverse wave in the refracted wave can be neglected. Therefore, there is only the refracted longitudinal wave P_{tz} outside the boundary of the plate notch AB. When the refracted longitudinal wave P_{tz} is transmitted to the CD boundary, in addition to the reflected longitudinal wave P_{fz} and the reflected transverse wave P_{fh} , a refracted longitudinal wave P'_{tz} is also generated. Since the two skew slots are parallel and the distance between the slots is much smaller than the wavelength, if the longitudinal waves are reflected at the notch, and the reflected waves include longitudinal waves and transverse waves, the output longitudinal wave normal stress σ_2 and the output shear stress τ_2 will be superimposed between the inclined slots, and the stress state at any micro-element in the notch is shown in Fig. 3.

According to Snell's law:

$$\frac{\sin\alpha}{V_{Pr}} = \frac{\sin\beta}{V_{P_{fh}}} = \frac{\sin\alpha}{V_{P_{fz}}} = \frac{\sin\alpha_t}{V_{P_{tz}}} \tag{3}$$

where α is the longitudinal wave incident angle (rad); β is the reflection angle of the reflected transverse wave (rad); and α_t is the transmission angle of the transmitted longitudinal wave (rad).

According to the physical conversion relationship between elastic wave velocity and medium parameters, it can be known as:

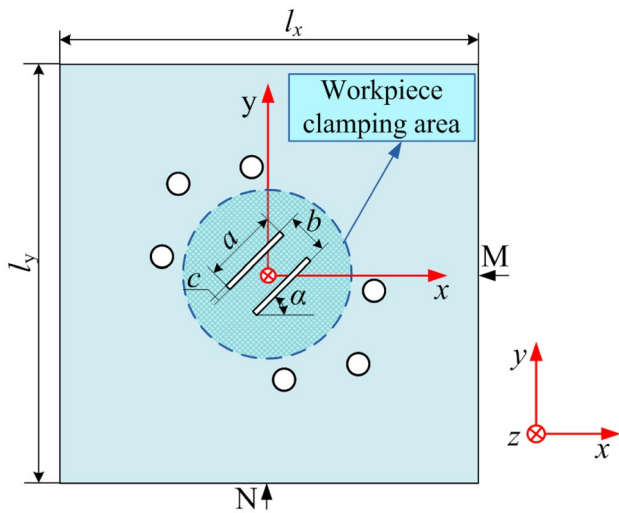


Fig. 1 Top plate of plate vibration device

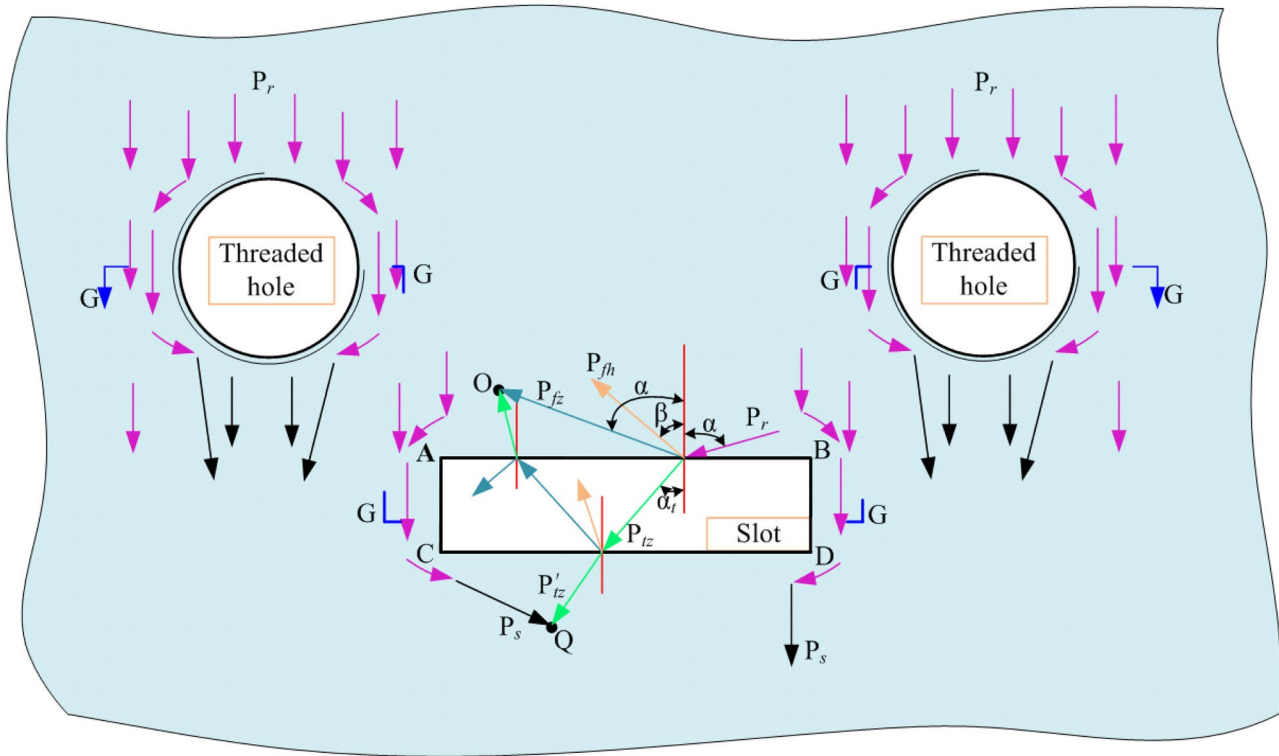


Fig. 2 Propagation of sound waves at the slot hole of a flat plate

$$\frac{\sin \alpha}{\sin \beta} = \frac{V_{pfz}}{V_{pfn}} = \sqrt{\frac{2(1 - \mu)}{1 - 2\mu}} \quad (4)$$

where μ is the Poisson’s ratio, V_{pfz} is the longitudinal wave sound velocity, and V_{pfn} is the transverse wave sound velocity.

It can be seen from Eq. (4) that the wave speed of the reflected longitudinal wave increases with the increasing of the inclination angle α , so changing the incident inclination angle can change the propagation characteristics of the longitudinal wave in the plate. The ultrasonic wave propagates through the slot and the hole and converges at the O point

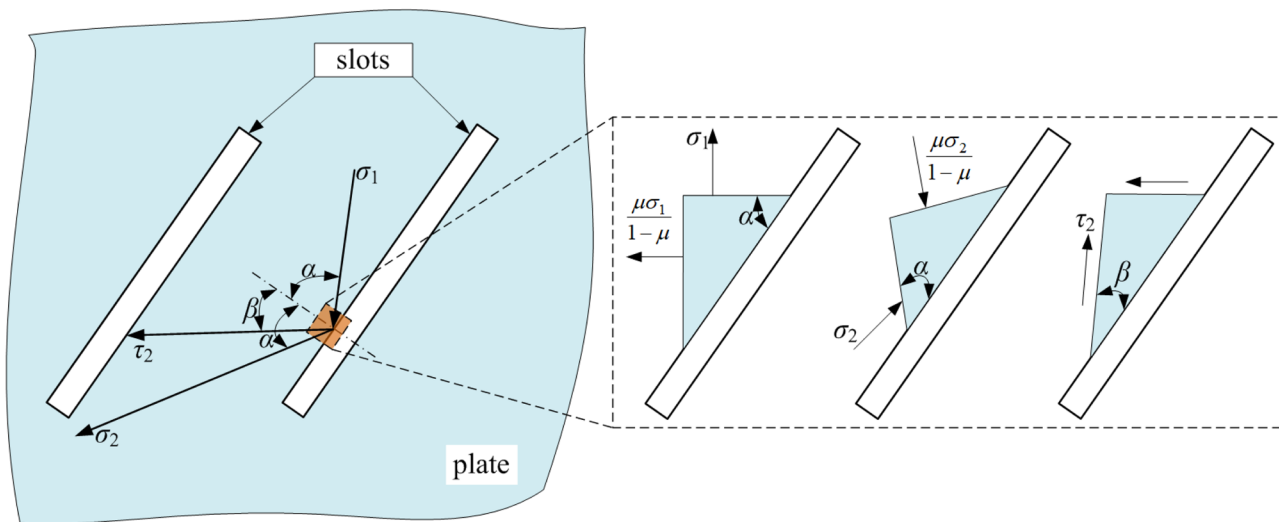


Fig. 3 Stress state of micro-element after longitudinal wave reflection

and **Q** point area. At point **Q**, there is a longitudinal wave P_{tz} refracted through the slot and a transverse wave P_s formed after refraction and reflection at the edge of the slot. The longitudinal wave P_{tz} and the composite of the transverse wave P_s form a torsional vibration perpendicular to the original longitudinal direction. The transmission of the transverse wave increases the vibration energy in the z direction and the displacement around these slots. Therefore, the reasonable distribution of slots and holes can help to change the propagation direction of internal waves in the plate, and then affect the vibration characteristics of the plate.

3 Composition of vibration platform

The plate vibration device is mainly composed of pedestal, columns, vibrating plate, and ultrasonic oscillators. Figure 4 shows the distribution of stress and amplitude of the vibration platform.

Ultrasonic excitation at 28,000 Hz was applied to the side points **M** and **N** of the plate in Fig. 1, and the inclination angle and width of the slot were changed to perform the finite element modal harmonic response analysis. The specific parameters are shown in Table 1.

3.1 Simulation results of the top vibrating plate

In order to study the vibration characteristics of the vibrating plate and the dynamic response under different frequency loads, this paper used ANSYS Workbench software to simulate and analyze the modal harmony response of the theoretically designed 28,000 Hz top vibrating plate by adjusting the slot inclination α and the width of the slot. Among them, the FEM results of a vibrating flat plate with a slot width of 2 mm are shown in Fig. 5. The cloud image

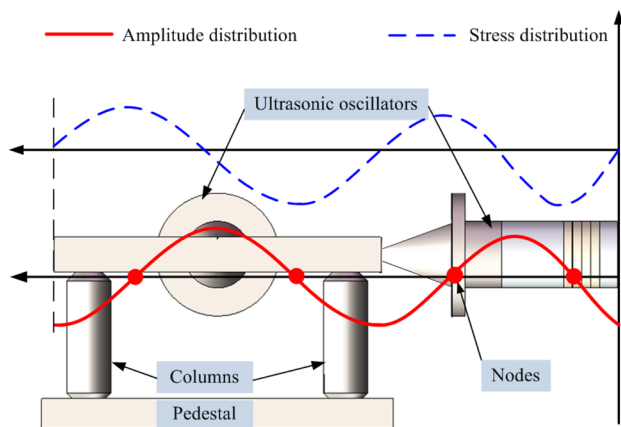


Fig. 4 Stress and amplitude distribution of vibration platform

of the flat plate after ultrasonic excitation shows a certain regular change, and the red area represents the position of the strongest vibration. Since it is desired to obtain a certain amplitude at the position where the workpiece is clamped during processing, the finite element analysis only pays attention to the vibration at the position where the vibrating plate is mounted on the workpiece.

Similarly, FEM analysis was carried out for vibrating plates with slot widths of 1 mm, 3 mm, and 4 mm. The histogram of simulation results is shown in Figs. 6 and 7. It can be clearly seen that when the slot width is 2 mm, the uniformity of both modal amplitude and harmonic response amplitude distribution is better than the other three groups. The main reason is that the refraction, reflection, and scattering phenomena occurred when the ultrasonic propagates at the slot position. According to the propagation law of sound wave, the refraction phenomenon does not change the frequency of the wave but changes the wavelength and wave velocity. The scattering phenomenon makes the sound wave propagate again after losing part of its energy at the slot. When the slot is too large, the energy lost by the sound wave is greater; if the slot is too small, the refraction phenomenon is not obvious, and it is difficult to form a new emission point where the sound waves are collected. Therefore, according to the simulation results, the slot width was determined to be 2 mm.

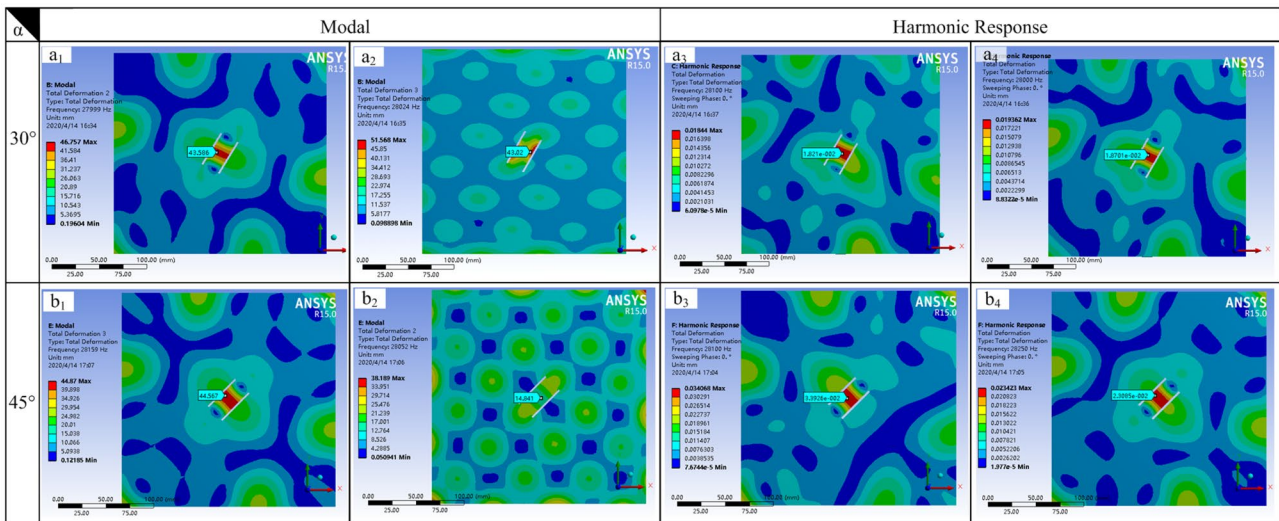
According to the relationship between the inclination angle and frequency of the slot in Fig. 8, when the slot width is 2 mm, the vibration frequencies with incident angles of 30° , 45° , and 150° approach the design frequency most, and the minimum deviation between the frequency with inclination angle of 45° and the designed 28,000 Hz value is 0.07%.

3.2 Simulation analysis of plate vibration device

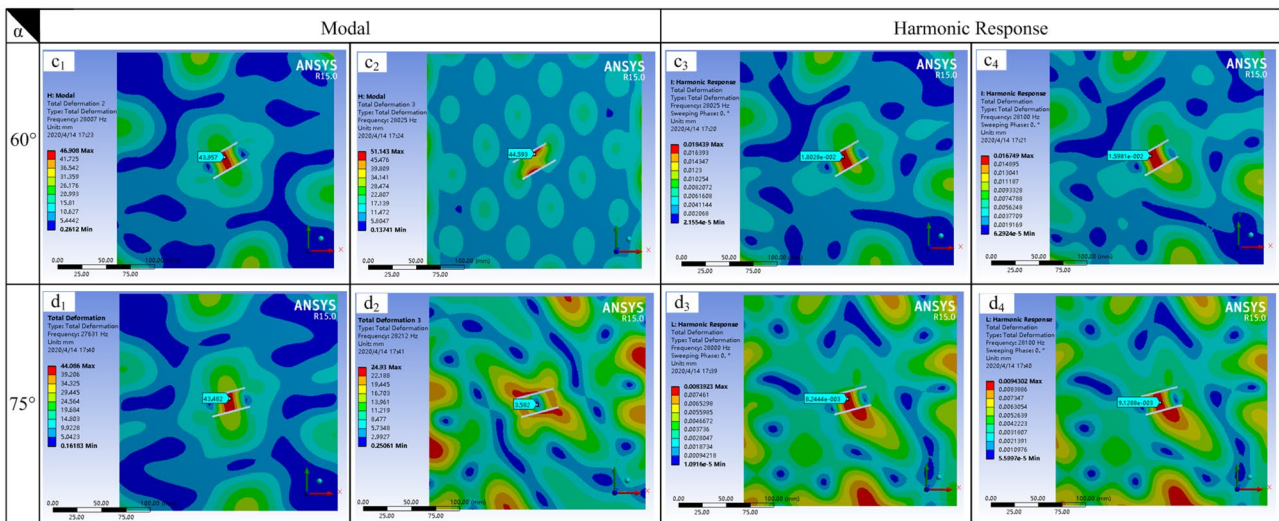
From the analysis results of the modal harmonic response of the vibrating plate, it can be seen that the dark blue position in the plate cloud chart indicates that the vibration is the weakest. This position is suitable for clamping and fixing the workpiece. Therefore, the workpiece fixing hole and pedestal positioning hole were set at the position with the lowest amplitude. After the assembly of the top panel and pedestal, the overall modal analysis and harmonic response analysis were carried out, the solidworks model (Fig. 9) was imported into the workbench for overall modal analysis and harmonic response analysis.

Table 1 Simulation parameters of vibrating plate

$\alpha/^\circ$	a/mm	c/mm	b/mm
30 45 60 75 115 135 150	40	1 2 3 4	20



a) Modal and harmonious response of slot with inclination angles of 30° and 45°



b) Modal and harmonious response analysis of slot with inclination angles of 60° and 75°

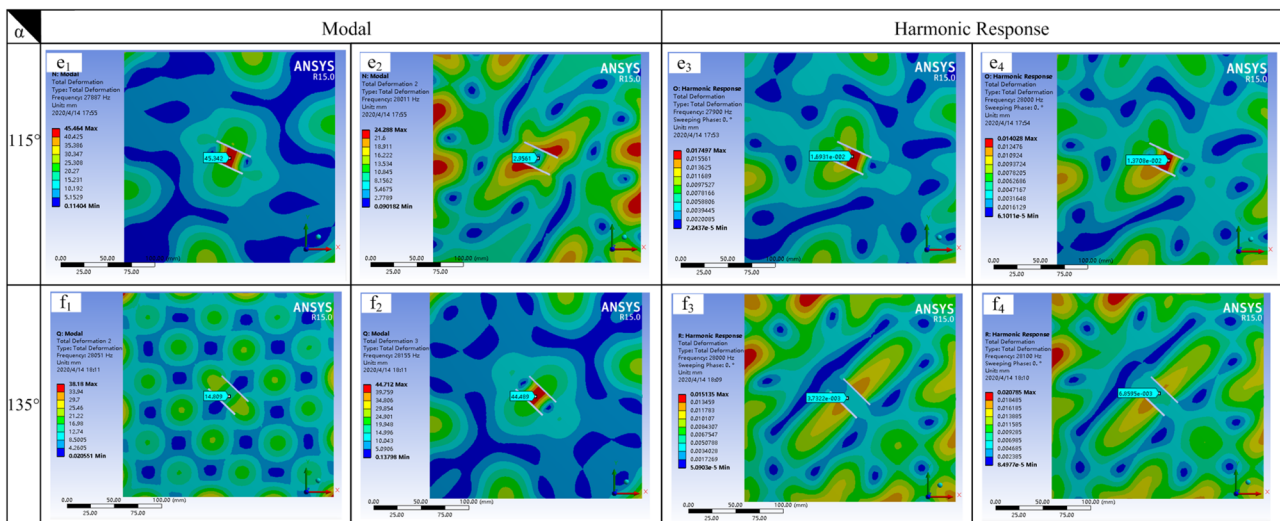
Fig. 5 FEM results of a vibrating plate with a slot width of 2 mm. a Modal and harmonious response of slot with inclination angles of 30° and 45°. b Modal and harmonious response analysis of slot with

inclination angles of 60° and 75°. c Modal and harmonious response analysis of slot with inclination angles of 115° and 135°. d Modal and harmonious response analysis of slot with inclination angles of 150°

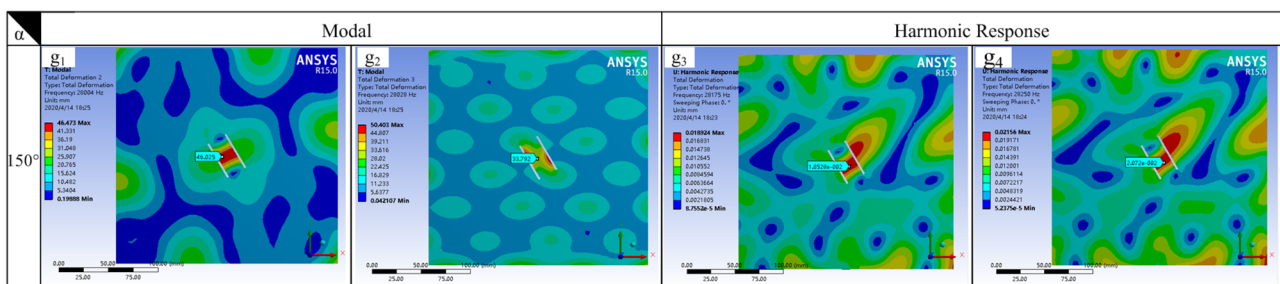
According to the actual processing conditions, the bottom plate of the vibration platform was fixed, and ultrasonic vibration excitation was applied to the end faces of the two horns, respectively. In order to improve the simulation efficiency, the tetrahedral structure was used for mesh division, as shown in Fig. 10. There were 79,668 mesh elements and 144,527 nodes, and the modal frequency range was set as 27,000 ~ 29,000 Hz. The overall vibration characteristics of the vibrating plate when the inclination is 30°, 45°, and 150°, as shown in Fig. 11. Compared with the cloud diagram of the simulation results, it was found that the vibration

effect of the top panel with the frequency of 27,600 Hz was the best when the inclination was 45°; the vibration effect of the top panel in other frequency ranges was not ideal. Therefore, it was preliminarily determined that the overall frequency of the vibration platform was 27,600 Hz, with a deviation of 0.14% from the 28,000 Hz in the theoretical design, which was mainly caused by the neglect of the non-uniformity of materials and the error of software mesh generation in the simulation calculation.

In order to quantify the platform vibration, the workbench software was used to simulate the amplitude along



c) Modal and harmonious response analysis of slot with inclination angles of 115° and 135°



d) Modal and harmonious response analysis of slot with inclination angles of 150°

Fig. 5 (continued)

the coordinate axis in three directions, as shown in Fig. 12, where $x-z$ is the amplitude along the z axis on the A_1-A_2 (path A) path and $y-z$ is the amplitude along the z axis on the B_1-B_2 (path B) path. The simulation results show that the amplitude is the largest at the position where the workpiece is installed in the middle of the platform, and the vibration in the vertical direction (i.e. z direction) is generated, which is in line with the previous analysis of the motion of sound waves in the flat plate (Sect. 2.2).

4 Amplitude test and cutting test of ultrasonic vibration plate

4.1 Plate vibration performance test

In the finite element analysis process of the plate vibration device, the dimensions of the ultrasonic vibration horn and the vibration platform are theoretical values, and the

material parameters are standard values selected according to the material characteristics. In fact, there are many uncertain factors in the preparation and processing of materials, which cause the final result to deviate from the ideal state. In order to verify the reliability of the theoretical design and simulation analysis, and to further study the vibration characteristics of the flat panel, it is necessary to conduct impedance analysis and amplitude testing of the basic performance of the flat panel vibration device.

1. Impedance analysis

The PV70A impedance analyzer was used to conduct impedance analysis on the processed flat vibration device. As shown in Fig. 13, it was found that the admittance roundness was good and has no parasitic circle. The value of the impedance, the resonance frequency, and the quality factor was 12.17Ω , 27,500 Hz, and 1266.8, respectively; these test results met the design requirements. Therefore, the errors

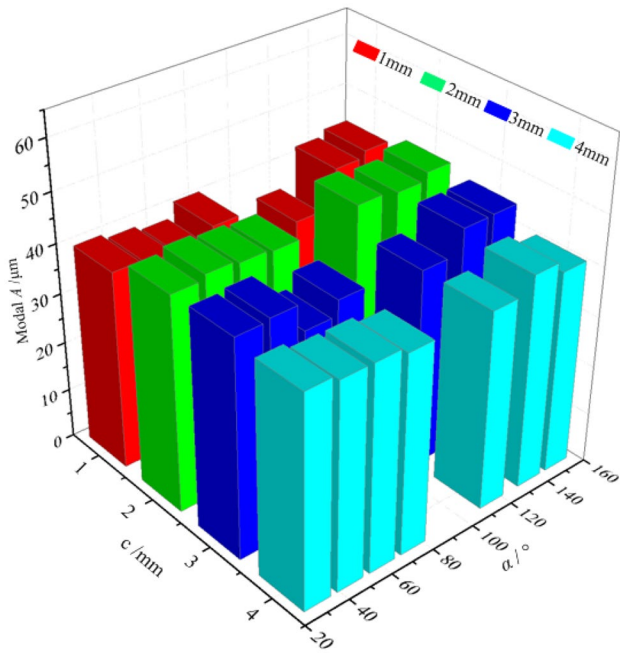


Fig. 6 The modal amplitude distribution corresponding to different slot widths

between the measured frequency and the results of theoretical calculation and finite element analysis are 1.78% and 0.36%, respectively.

The 28,000-Hz ultrasonic generator was connected to the plate vibration device, and the LK-G10 laser displacement

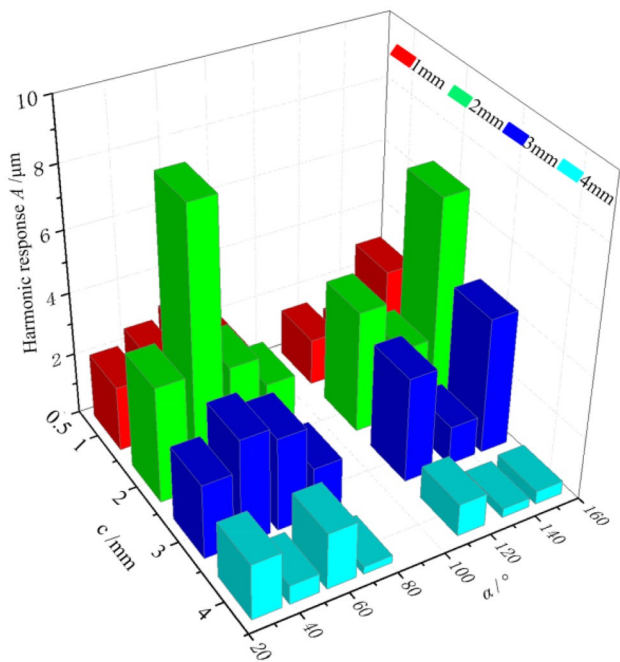


Fig. 7 Harmonic response amplitude distribution corresponding to different slot widths

sensor was used to test the amplitude of the vibration platform. The measured maximum amplitude of the area where the workpiece is installed on the vibration platform is 8 μm. After processing the test data, the motion track of any point in the area where the workpiece is installed is a spatial ellipse, as shown in Fig. 14, indicating that there is an upward vibration component in the position area; that is to say, the slot changes the propagation direction of ultrasonic wave in the plate.

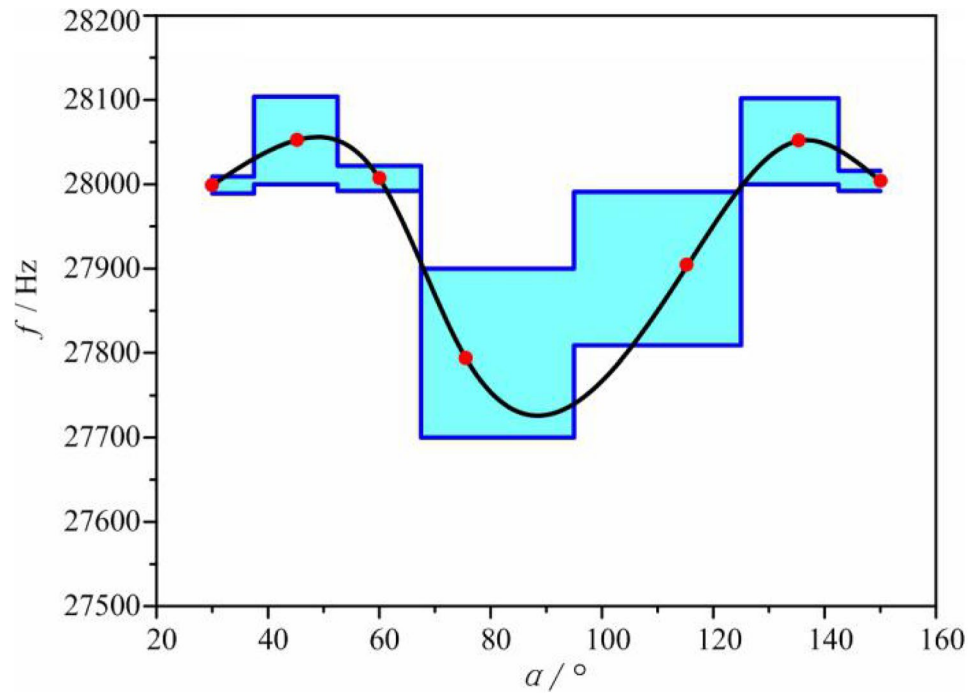
It can be seen from Fig. 14 that after ultrasonic vibration is applied to the platform with a 45° slot, a multi-directional simple harmonic vibration with a certain amplitude can be realized at any point near the center of the vibrating plate. Since ultrasonic vibration cannot be observed by human vision, in the test of ultrasonic vibration effect, the atomization phenomenon or sand jumping phenomenon on the radiation surface of vibrating body are often used to observe the macro performance of vibration. By dropping water on the side of the plate to observe its vibration, it was found that under the action of ultrasonic high-frequency vibration excitation, when the power frequency was adjusted to near the resonance point, obvious atomization occurred on both sides of the plate (Fig. 15), indicating that there was a strong ultrasonic longitudinal vibration on the side of the plate. A layer of fine sand particles was evenly scattered on the top of the plate. After vibration, the sand particles were scattered and finally stabilized. It was found that the sand particles on the surface of the plate were redistributed. The position with sand particles was the depressed point, and there was no sand particles in the position of the workpiece installed on the surface of the plate (Fig. 16), indicating that the slot changed the propagation direction of ultrasonic longitudinal vibration, and the vibration of the vertical component was generated.

4.2 Test conditions

The Ti2AlNb intermetallic alloy, a difficult-to-process aerospace material, was selected for the experiment, and its chemical composition is shown in Table 2. Combined with the self-developed ultrasonic tool holder, the plate vibration device was fixed to the machine tool station, and the Ti2AlNb intermetallic alloy was subjected to ultrasonic vibration milling experiments on a three-axis vertical machining center, so as to study the impact of the vibration characteristics of the vibration platform on the cutting process. The test site is shown in Fig. 17, and the test conditions are shown in Table 3. Besides, the vibration of machining center was ignored in actual processing.

Ultrasonic vibration excitation was applied along the tool feed direction and radial direction. The main factors affecting cutting performance are spindle speed, ultrasonic amplitude, feed rate, and depth of cutting. This experiment took the spindle speed and the amplitude of the plate vibration device as the research object. The single factor test was designed to study the influence of the

Fig. 8 Modal frequency distribution of 2-mm slot width



vibrating plate on the cutting performance of the workpiece. The test parameters are listed in Table 4.

5 Experimental results and discussion

5.1 Surface topography

5.1.1 The influence of speed on surface topography

The surface quality of the workpiece and the changes in chip breaking and chip morphology were used to reversely characterize the cutting performance of the

workpiece. Figures 18, 19, 20, 21, 23 and 24 showed the surface topography of the workpiece under different parameters observed under the white light interferometer. It can be seen that there were obvious differences between the surface topography obtained by ultrasonic vibration cutting and common cutting. The surface topography after ultrasonic vibration cutting showed stronger regularity and artistic beauty. Due to the special mechanical properties of workpiece materials, there were also great differences between the results after the 2DUVC

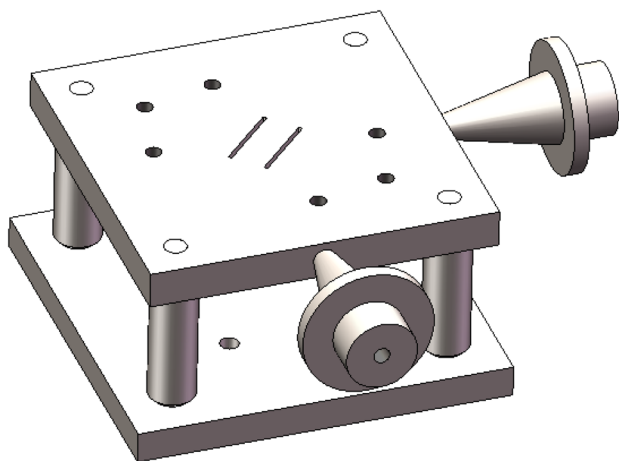


Fig. 9 Modeling of the slot-type vibration platform

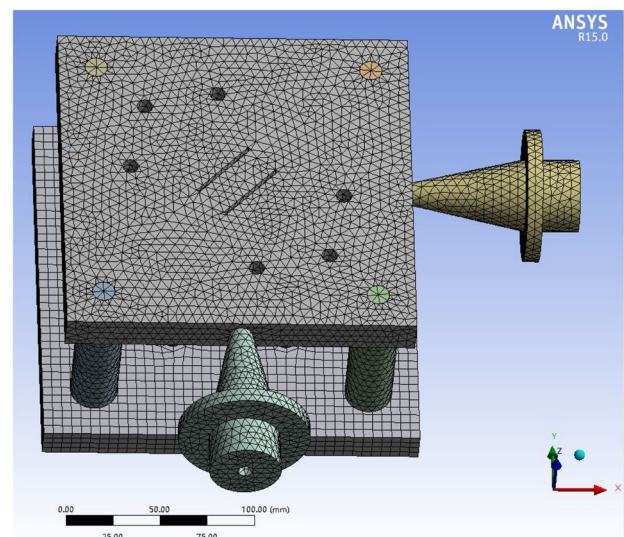


Fig. 10 Meshing diagram

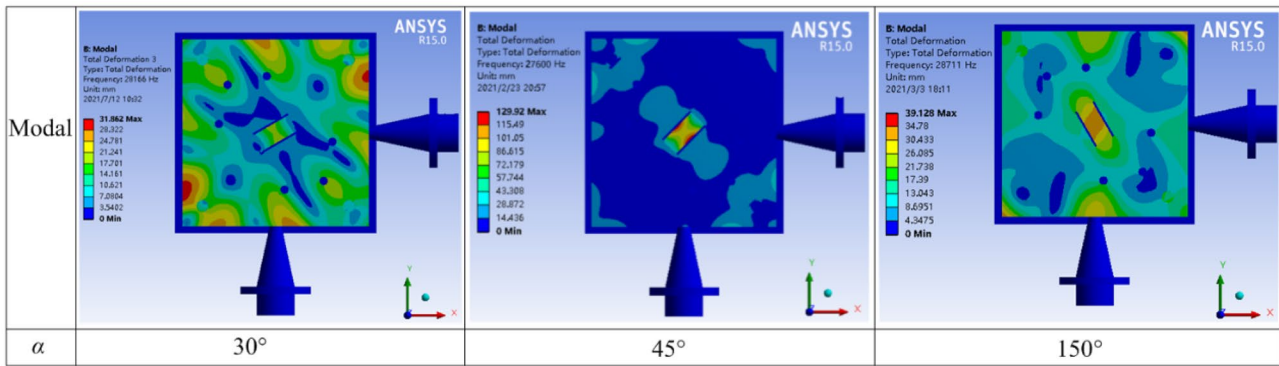


Fig. 11 Overall modal analysis of 2-mm slot width

and 3DUVC. When the spindle speed was 1700–3100 r/min, the surface topography processed by the plate vibration device was a unique “drainage tank” (as shown in Fig. 20), which is very similar to the hydrophobic tiles on the roof of Chinese classical buildings. This microstructure topography is conducive to the use of the workpiece surface in special occasions. The research showed that the regular micro-texture on the surface of the friction pair not only reduces the actual contact area between the surfaces of the friction pair but also realizes the storage of lubricating fluid, which can effectively reduce friction, reduce wear, and improve the bearing capacity [42]. Bionics and tribology research showed that the material with surface texture has better friction reduction

and wear resistance [43, 44]. The similar microstructure was obtained by 3DUVC at the speed of 3100 r/min, but its roughness value was about 15.2% higher than that of 2DUVC. The topography of CC was relatively poor, and there was a certain degree of scratch. It was found from the histogram in Fig. 22 that the surface roughness value obtained after the processing of the flat-plate vibration device was relatively small, and when the spindle speed was 1700 r/min, the roughness value of 2DUVC was 54% and 57% lower than that of 3DUVC and CC, respectively. Therefore, when the spindle speed was 1700 r/min, the designed flat-plate vibration device exhibited better vibration characteristics under the condition of only two-dimensional ultrasonic longitudinal excitation.

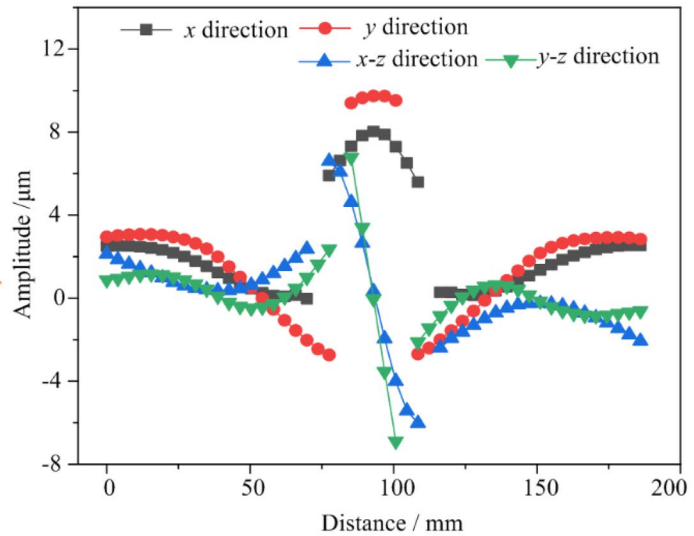
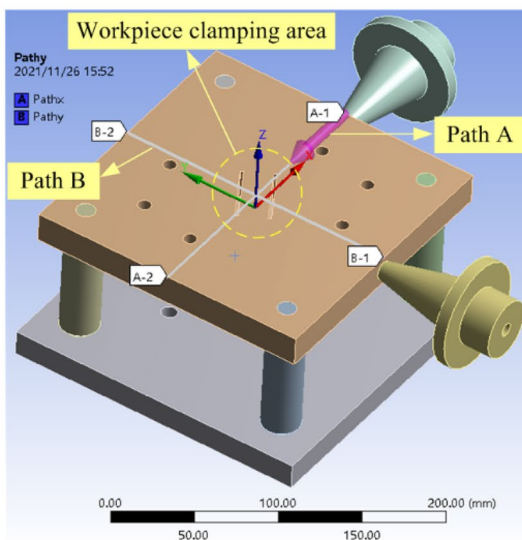


Fig. 12 Overall modal analysis of 2-mm slot width

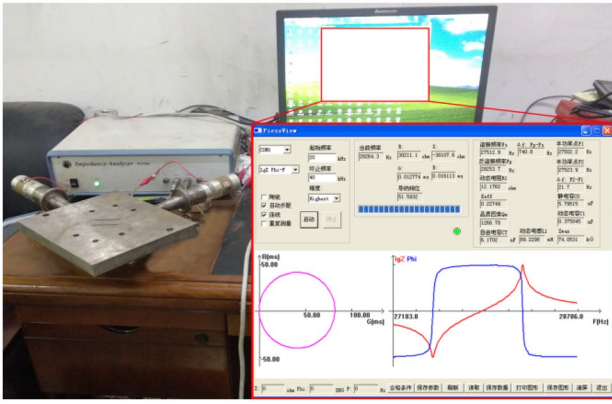


Fig.13 Impedance test site and results

Therefore, compared with CC process, ultrasonic vibration cutting can obtain better surface morphology. 2DUVC process can obtain certain micro-texture when the spindle speed was 1000–3100 r/min, but the micro-texture morphology was the best when the speed was 1700 r/min, and then the quality of surface morphology became worse with the increase of speed. The spindle speed was closely related to the cutting speed. When the cutting speed was low (i.e., the speed was 1000–2400 r/min, as shown in Fig. 19a–c), the micro-texture morphology of 3DUVC was not obvious and the quality was poor. When the cutting speed was high (i.e., the speed was 3100 r/min, as shown in Fig. 19d), the obvious micro-texture morphology can be obtained, but when the cutting speed was high, the separation characteristics

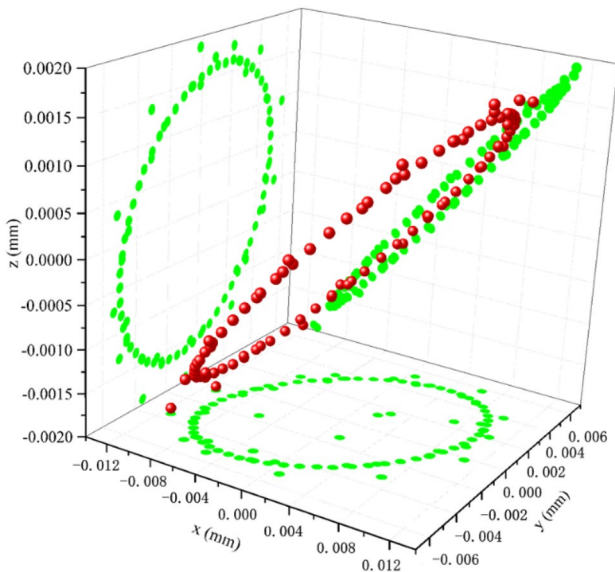


Fig. 14 Movement track of a point in the center of the platform

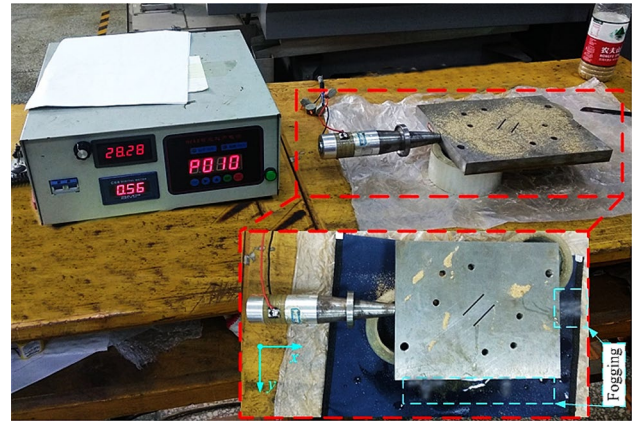


Fig. 15 Atomization effect of platform

of ultrasonic vibration were weakened; therefore, the obtained surface roughness value was larger.

5.1.2 The influence of amplitude on surface topography

According to the effect of machine speed on surface roughness, the influence of vibration platform amplitude on surface quality was studied when the spindle speed was 1700 r/min, the feed speed was 210 mm/min, and the cutting depth was 0.1 mm (where A_x was 6 μ m, refer to Figs. 18 and 19, and the appearance of common cutting, refer to Fig. 21). The test results in Figs. 23, 24 and 25 show that the surface after ultrasonic vibration cutting showed a more delicate surface topography, and the micro-texture topography was more obvious when the amplitude was relatively small. Since the radial direction is perpendicular to the direction of movement of the tool, in this direction, the tool is always in contact with the workpiece material, so the edge of the microstructure of the workpiece is continuous

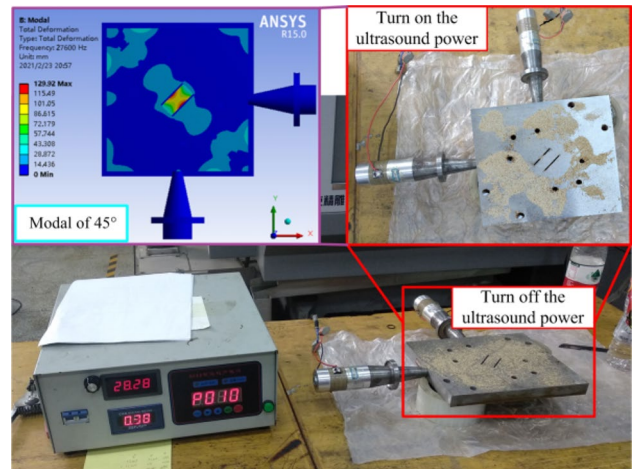


Fig. 16 Sand vibration effect of platform

Table 2 Chemical composition of the Ti₂AlNb alloy (wt%)

Al	Nb	Mo	Fe	Si	C	Ti
10.0	41.4	0.9	0.05	0.03	0.12	Bal

in the radial direction. The vibration in the feed direction is parallel to the moving direction of the tool. The ultrasonic vibration in this direction promotes the separation of the workpiece material and the matrix, and the cutting edge contacts the workpiece material periodically. When the amplitude is large, the ultrasonic impact is strong. Therefore, the overall topography after machining is in the shape of high and low undulating gullies along the feed direction. Compared with the results of CC, the surface fluctuation after 2DUVC was smaller, which indicated that the workpiece was subjected to vertical upward reaction during cutting, so that the slot edge of the workpiece surface was ironed and the surface roughness was reduced. It verified the theoretical analysis and simulation results of vertical vibration at the slot position in this paper. The topography of 3DUVC and CC was random and had no strong regularity. The analysis reason was that the 3DUVC in this test had one more longitudinal vibration along the tool axis than the 2DUVC. After the vibration in the vertical direction of the vibration platform was superimposed

Table 3 Test conditions

Key parameters	Numerical value
Tool diameter <i>d</i> / mm	8
Tool material/type	WC/Bull nose milling cutter
Tool longitudinal vibration frequency <i>f</i> ₁ /Hz	35,000
Tool longitudinal vibration amplitude <i>A</i> ₁ /μm	8
Platform vibration frequency <i>f</i> ₂ /Hz	28,000
Platform longitudinal vibration amplitude <i>A</i> _x /μm	2 4 6 8
Platform longitudinal vibration amplitude <i>A</i> _y /μm	1.6 3.2 4.8 6.4
Workpiece material	Ti2AlNb intermetallic alloy
Cutting type	Dry
Ultrasonic vibration dimension	0(CC) 2(2DUVC) 3(3DUVC)

in this direction, it had a large impact on the machined surface of the workpiece; the surface topography of the workpiece was destroyed by this impact force to a certain extent. It can be seen from the histogram in Fig. 25 that among the three processing processes, the surface roughness of the workpiece after 2DUVC processing was lower, and its surface roughness value was the smallest when the amplitude was 8 μm along the feed direction, which was

Fig. 17 Test site

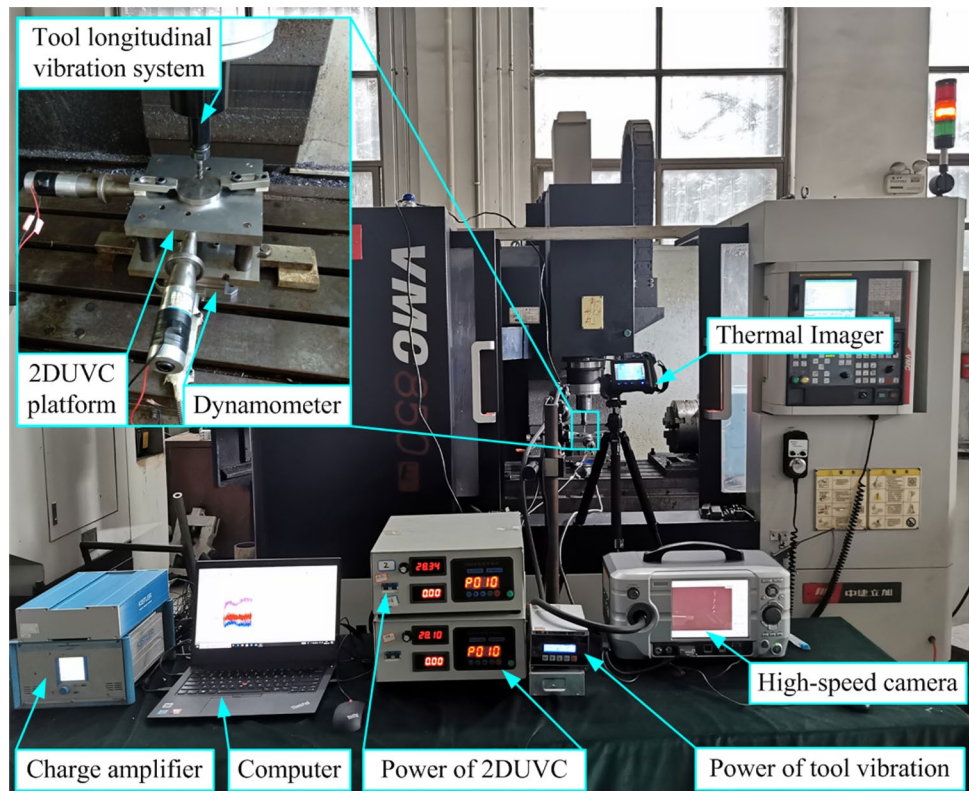


Table 4 Single-factor test cutting parameters

Spindle speed <i>n</i> /(r/min)	Longitudinal vibration amplitude of platform		Depth <i>a_p</i> /mm	Tool longitudinal vibration amplitude <i>A₁</i> /μm
	<i>A_x</i>	<i>A_y</i>		
1000 1700 2400 3100	0	0	0.1	8
	6	4.8		
1700	0	0	0.1	0.8
	2	1.6		
	4	3.2		
	6	4.8		
	8	6.4		

about 64% and 65.9% lower than that of 3DUVC and CC, respectively. This was mainly due to the increase of the amplitude in the feed direction, the increase of the separation characteristics between the tool and the workpiece along the feed direction, the shortening of the net cutting

time, the periodic participation of the cutting edge in cutting, the improvement of the heat dissipation in the cutting area, and the reduction of the formation of chip buildup to a great extent; thereby, the quality of the machined surface was improved. Therefore, when the spindle speed and feed speed are determined, the vertical amplitude within a certain range is helpful to improve the vibration characteristics of the vibration platform.

According to the roughness value obtained from variable amplitude cutting test, the expression of the relationship between amplitude and surface roughness in 2DUVC and 3DUVC were obtained as Eqs. (5) and (6), respectively; the formulas can be used to predict the influence of ultrasonic amplitude on surface roughness.

$$Ra = (-0.00531 \pm 0.00254)A^2 + (0.04327 \pm 0.002584)A + (0.21425 \pm 0.05665) \tag{5}$$

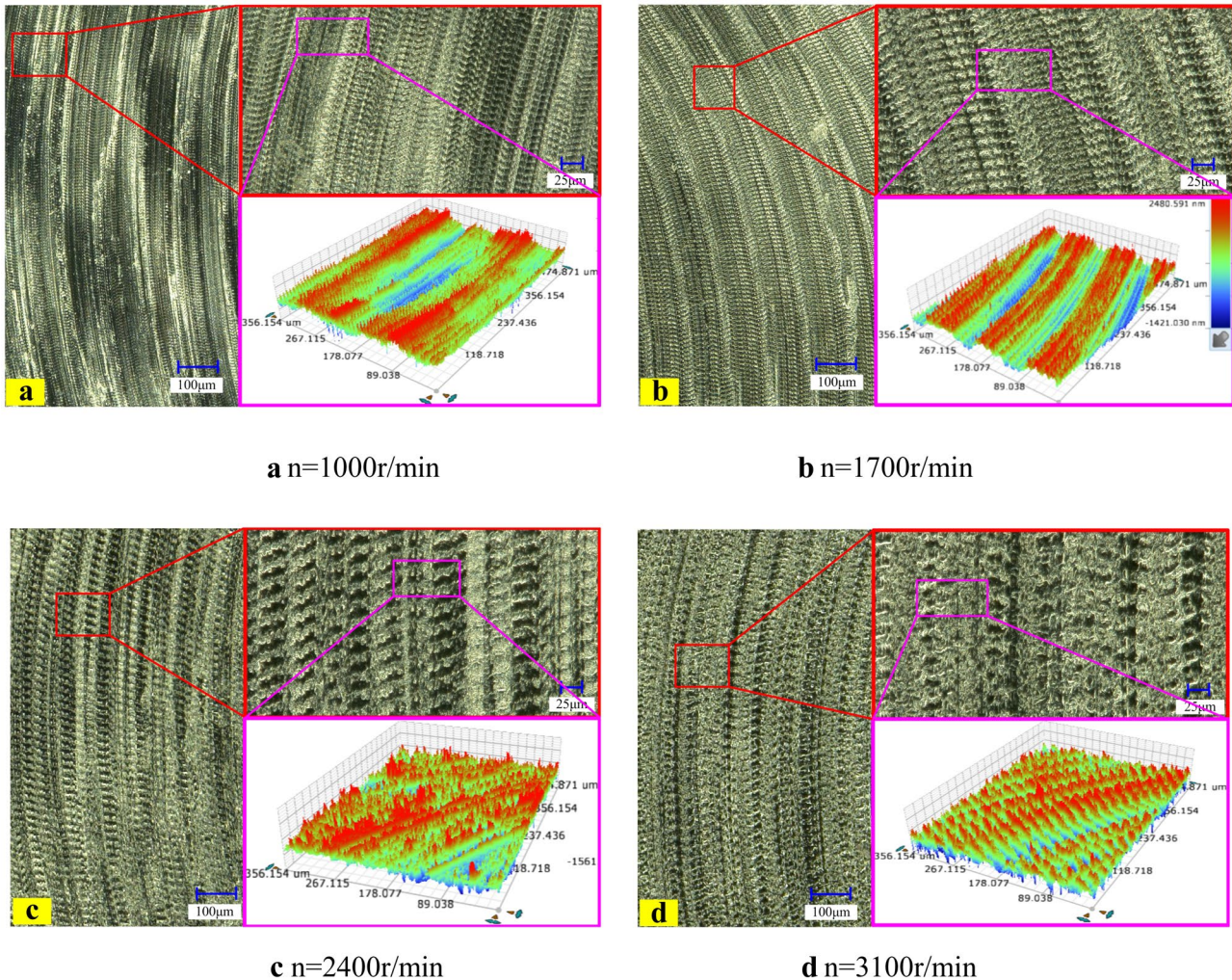


Fig. 18 Surface topography of 2DUVC. **a** *n* = 1000 r/min. **b** *n* = 1700 r/min. **c** *n* = 2400 r/min. **d** *n* = 3100 r/min

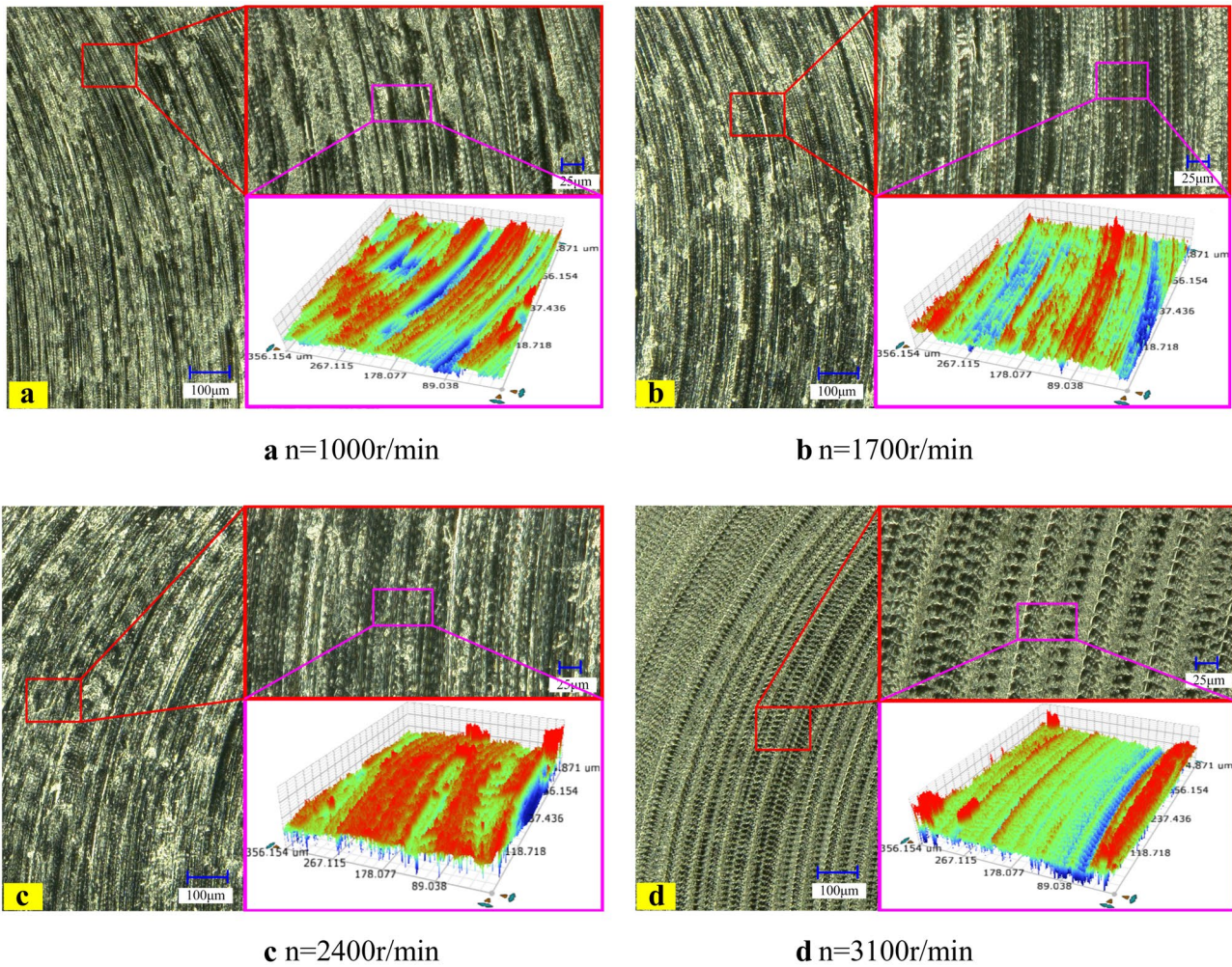


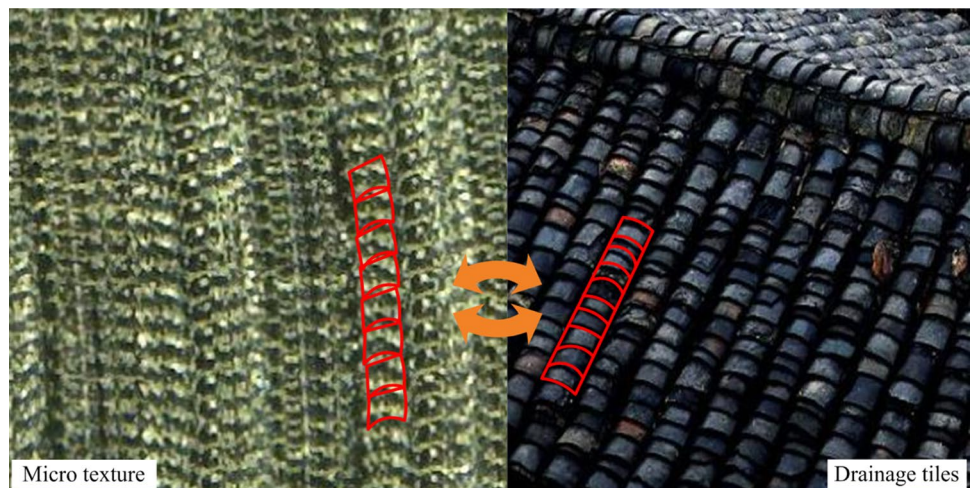
Fig. 19 Surface topography of 3DUVC. **a** $n = 1000 \text{ r/min}$. **b** $n = 1700 \text{ r/min}$. **c** $n = 2400 \text{ r/min}$. **d** $n = 3100\text{r/min}$

$$Ra = (-0.0005625 \pm 0.00204)A^2 + (0.03717 \pm 0.02073)A + (0.37125 \pm 0.04544) \tag{6}$$

5.2 Chip morphology

In the process of cutting, the change of chip length represents the difficulty of chip breaking of workpiece material,

Fig. 20 Micro-texture of 2DUVC



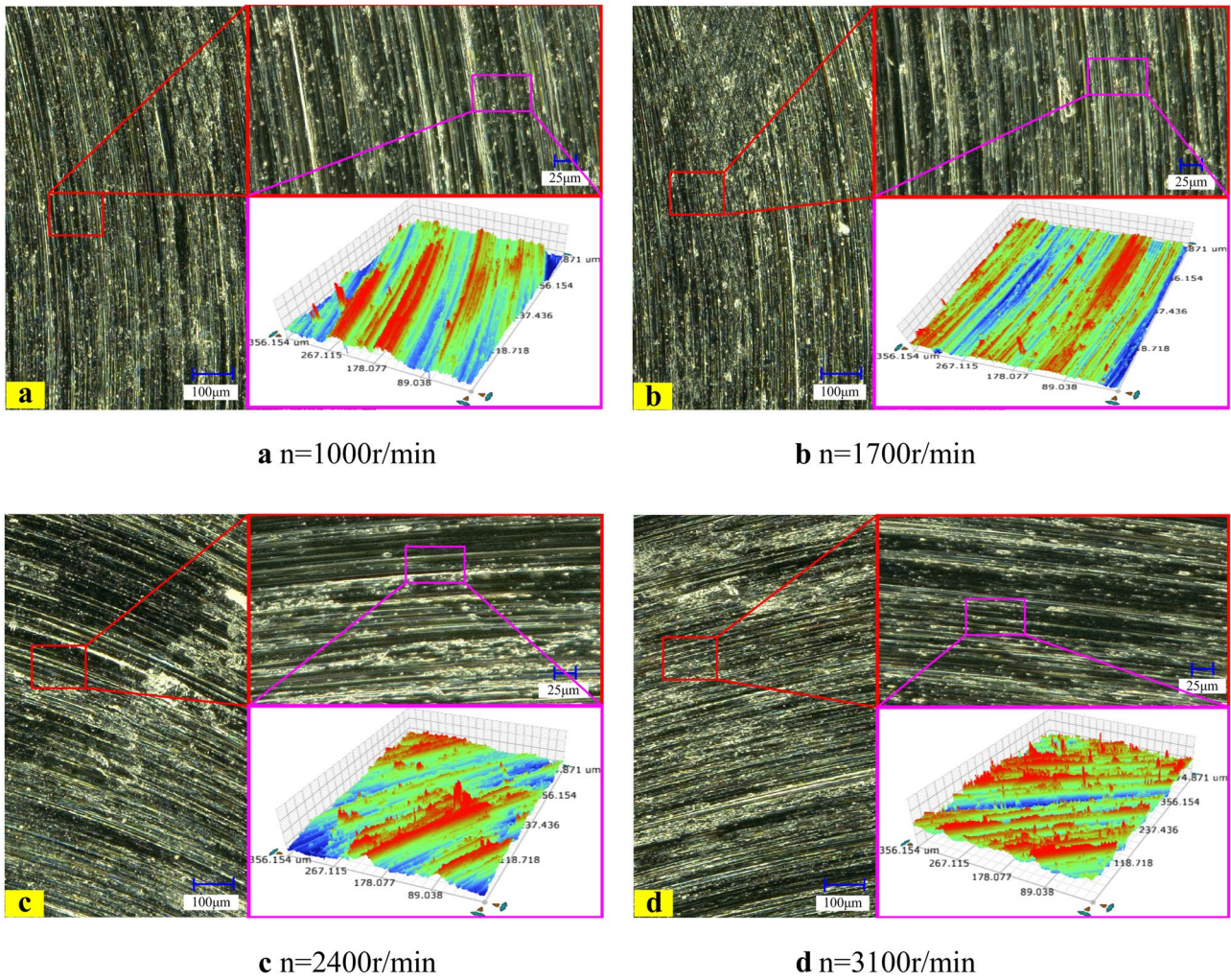


Fig. 21 Surface topography of CC. **a** $n = 1000$ r/min. **b** $n = 1700$ r/min. **c** $n = 2400$ r/min. **d** $n = 3100$ r/min

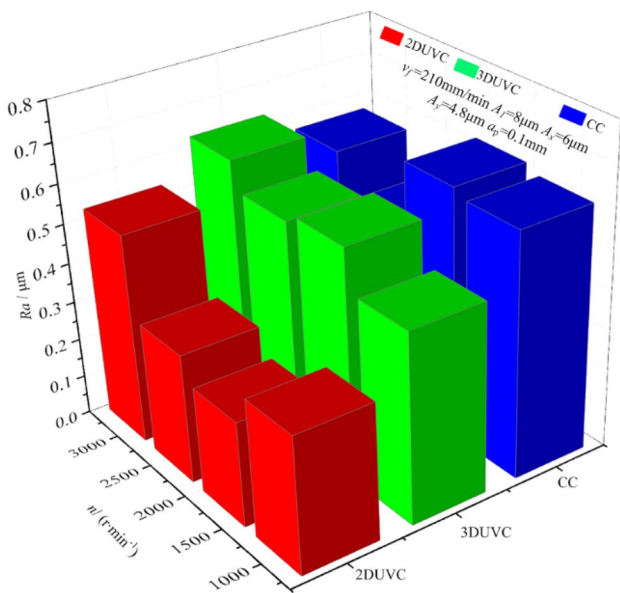
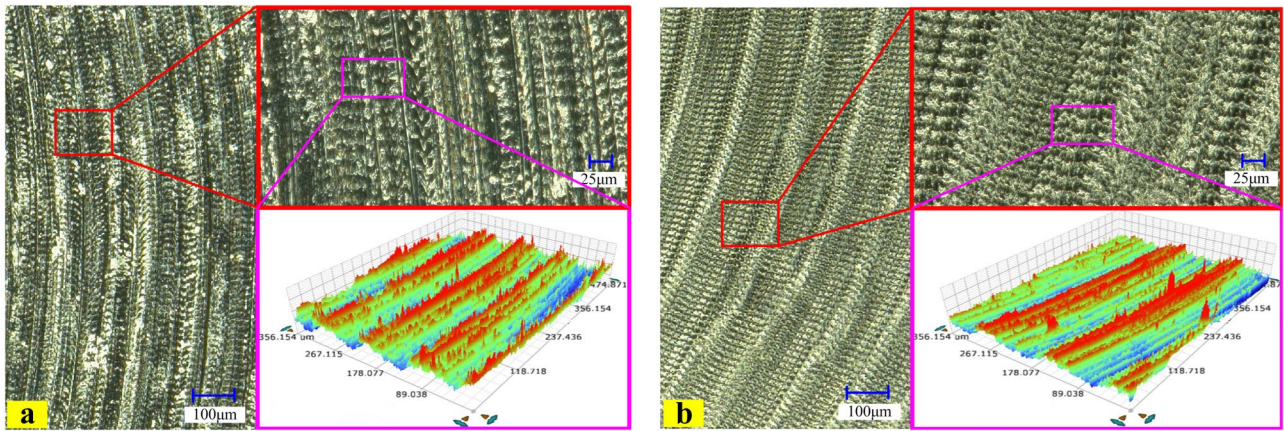


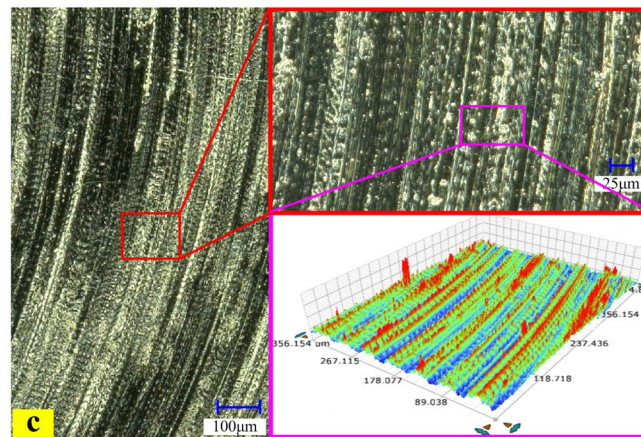
Fig. 22 Rotation speed-surface roughness change graph

which can be used as one of the judgment conditions of cutting performance of workpiece material. Based on the research on the influence of machine speed and plate amplitude on surface quality in this experimental, the number of sawteeth at the edge of chip with the same length was selected as the statistical object when the spindle speed was 1700 r/min, the feed speed was 210 mm/min, and the cutting depth was 0.1 mm. The experimental results are shown in Fig. 26, the influence of vibration platform on the cutting performance of Ti2AlNb intermetallic alloy is studied. Due to the excitation effect of ultrasonic vibration, in the cutting process, the workpiece material is not only subjected to the extrusion force of the tool rake face and the friction force of the tool rake face, but also subjected to the high-frequency impact force of ultrasonic vibration. In the process of chip formation, ultrasonic vibration accelerates the deformation of the cutting layer material to produce multiple stress concentration points, and many “tear zones” are formed at the stress



a $A_x=2\mu\text{m}, A_y=1.2\mu\text{m}, A_1=8\mu\text{m}$

b $A_x=4\mu\text{m}, A_y=3.2\mu\text{m}, A_1=8\mu\text{m}$



c $A_x=8\mu\text{m}, A_y=6.4\mu\text{m}, A_1=8\mu\text{m}$

Fig. 23 Surface topography of 2DUVC. **a** $A_x=2\mu\text{m}, A_y=1.2\mu\text{m}, A_1=8\mu\text{m}$. **b** $A_x=4\mu\text{m}, A_y=3.2\mu\text{m}, A_1=8\mu\text{m}$. **c** $A_x=8\mu\text{m}, A_y=6.4\mu\text{m}, A_1=8\mu\text{m}$

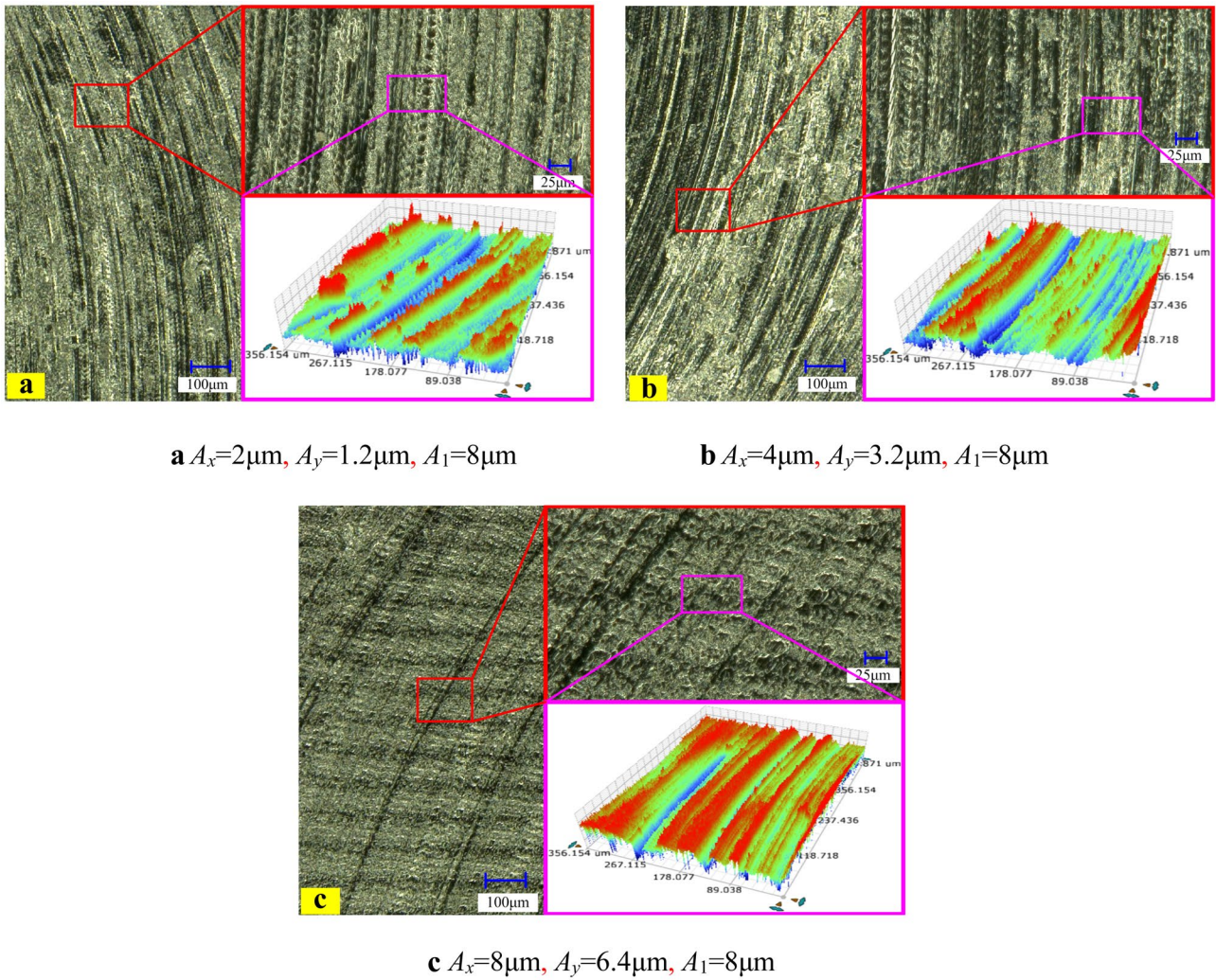


Fig. 24 Surface topography of 3DUVC. **a** $A_x=2\ \mu\text{m}, A_y=1.2\ \mu\text{m}, A_1=8\ \mu\text{m}$. **b** $A_x=4\ \mu\text{m}, A_y=3.2\ \mu\text{m}, A_1=8\ \mu\text{m}$. **c** $A_x=8\ \mu\text{m}, A_y=6.4\ \mu\text{m}, A_1=8\ \mu\text{m}$

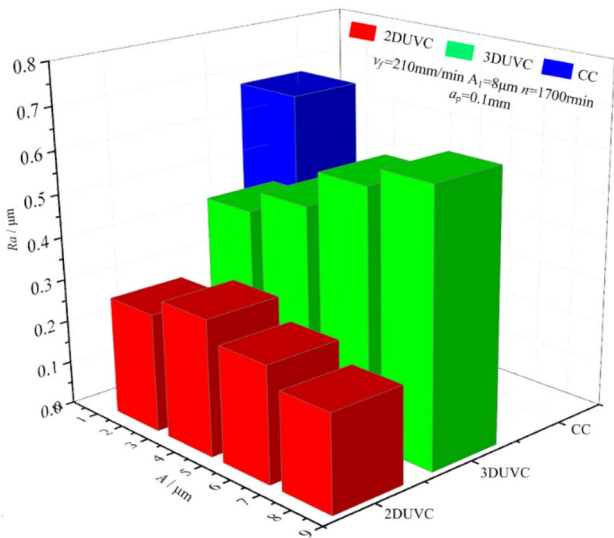


Fig. 25 The effect of amplitude on surface topography

concentration points. The macroscopic performance is the sawtooth phenomenon at the edge of the chip, and the chip is easy to separate and fracture from the matrix material at the sawtooth.

The number of serrations on the chip edge reflects the degree of deformation and the ease of chip breaking when the material is removed. The distribution of the number of chip sawteeth with equal length after the three cutting processes is shown in Fig. 27. The results showed that the sawtooth number generated by ultrasonic vibration cutting is more than that generated by common cutting, and with the increase of ultrasonic amplitude and vibration dimension, the sawtooth number also showed an increasing trend, it showed that 3D ultrasonic vibration cutting was easier to remove material. To a certain extent, it also confirmed the effect of speed and amplitude on surface quality under the same conditions in this experiment.

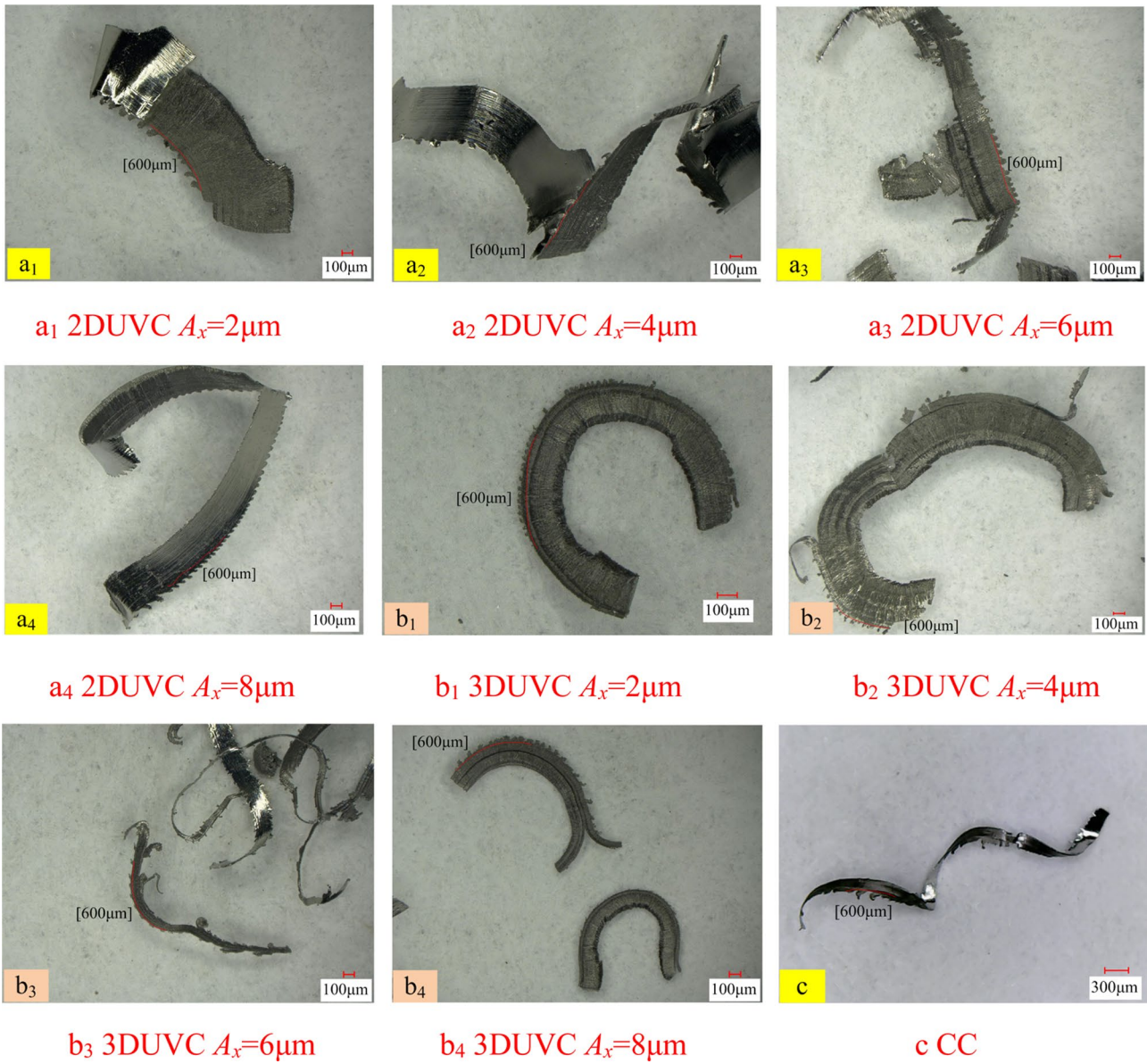


Fig. 26 Number of saw teeth of equal length chip after cutting by three processes. a₁ 2DUVC $A_x=2\mu\text{m}$. a₂ 2DUVC $A_x=4\mu\text{m}$. a₃ 2DUVC $A_x=6\mu\text{m}$. a₄ 2DUVC $A_x=8\mu\text{m}$. b₁ 3DUVC $A_x=2\mu\text{m}$. b₂ 3DUVC $A_x=4\mu\text{m}$. b₃ 3DUVC $A_x=6\mu\text{m}$. b₄ 3DUVC $A_x=8\mu\text{m}$. c CC

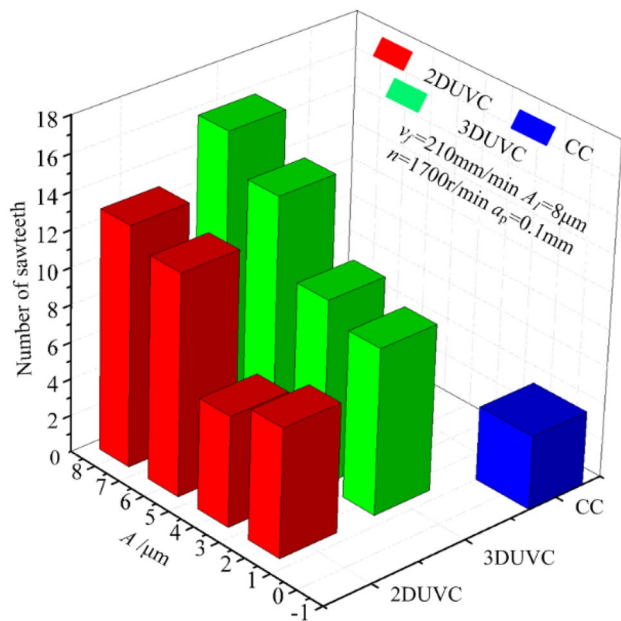


Fig. 27 The number of saw teeth of equal length after cutting by three processes

6 Conclusions

In order to solve the problems existing in the precision machining of typical difficult-to-machine materials (Ti2AlNb alloy), a two-dimensional ultrasonic vibration platform was designed by using the apparent elasticity method. The two-dimensional ultrasonic vibration platform was developed by combining theoretical design with finite element simulation and experimental study. The vibration characteristics of the platform were verified and studied by analyzing the surface quality and chip morphology after machining in CC and ultrasonic vibration cutting tests. The following conclusions were obtained based on the test process and test results:

1. According to the propagation characteristics of waves in different media, the influence of slot on the propagation path of waves in the flat plate was theoretically analyzed. The vibration characteristics of the vibration platform were simulated by the finite element software. The reliability of theoretical analysis was verified by vibration test and cutting test.
2. Compared with 3DUVC and CC, the cutting results of the vibration platform showed an obvious “drainage tank” microstructure in variable speed cutting. At 1700 r/min, the roughness value of 2DUVC decreased by 54% and 57% compared with that of 3DUVC and CC, respectively, so the 2DUVC showed better cutting characteristics. During variable-amplitude cutting, when

the amplitude in the feeding direction was 8 μm , the surface roughness value of 2DUVC was about 64% and 65.9% lower than that of 3DUVC and CC, respectively. According to the experimental data, the expression of the relationship between the amplitude of 2DUVC and 3DUVC and the surface roughness value was fitted, which can be used to predict the surface roughness value of the two processing technologies.

3. Under appropriate machining conditions, the machining results of 2DUVC of workpiece were better than other two machining processes, indicating that the plate vibration device exhibited better vibration characteristics under these conditions, while 3DUVC made it easier to remove materials, which is helpful for the promotion and application of multi-dimensional ultrasonic vibration cutting technology in high-precision fields of difficult-to-machine materials, and expands the application scope of ultrasonic vibration cutting technology.

Author contribution Zhaojie Yuan: Writing original draft, editing and experimental research. Guofu Gao: Conceptualization, review. Yi Wang: FEM analysis. Zongxia Fu: Experimental research. Daohui Xiang: Supervision.

Funding This research was supported by the National Natural Science Foundation of China (No.51875179).

Availability of data and materials The datasets used or analyzed during the current study are available from the corresponding author on reasonable request.

Declarations

Ethical approval The authors state that this paper is an original work, it has not been published in any journals, and this research does not involve any ethical issues of humans or animals.

Consent to participate The authors declare that this research involves no human participants and/or animals.

Consent for publication The authors confirm:

the paper described has not been published before that it is not under consideration for publication elsewhere that its publication has been approved by all co-authors that its publication has been approved by the responsible authorities at the institution where the work is carried out The authors agree to publish it in the Journal indicated below and also to publish the article in English by Springer in Springer’s corresponding English-language journal.

The copyright to the English-language article is transferred to Springer effective if and when the article is accepted for publication. The author warrants that his/her contribution is original and that he/she has full power to make this grant. The author signs for and accepts responsibility for releasing this material on behalf of any and all co-authors. The copyright transfer covers the exclusive right to reproduce and distribute the article, including reprints, translations, photographic reproductions, microform, electronic form (offline, online), or any other reproductions of similar nature.

Conflict of interest The authors no competing interests.

References

- Zhang HY, Yan N, Liang HY et al (2021) Phase transformation and microstructure control of Ti₂AlNb-based alloys: a review. *J Mater Sci Technol* 80:203–216. <https://doi.org/10.1016/j.jmst.2020.11.022>
- He LJ, Su HH, Xu JH et al (2018) Inverse identification of constitutive parameters of Ti 2 AlNb intermetallic alloys based on cooperative particle swarm optimization. *Chin J Aeronaut* 31(8):1774–1785. <https://doi.org/10.1016/j.cja.2018.01.002>
- Sim KH, Zhang F, Wang G et al (2017) Experimental comparison of ground surface characteristics for P/M Ti₂AlNb-based alloy using CBN and diamond grinding wheels. *Int J Adv Manuf Technol*. <https://doi.org/10.1007/s00170-017-0900-2>
- Ma XD, Xu JH, Ding WF et al (2013) Wear behavior of Ti(N, C)-Al₂O₃ coated cemented carbide tools during milling Ti₂AlNb-based alloy. *Key Eng Mater* 589–590:361–365. <https://doi.org/10.4028/www.scientific.net/KEM.589-590.361>
- Gao GF, Yuan ZJ, Xia ZW et al (2021) Study on thrust force of ultrasonic-assisted vibration micro-hole drilling of titanium alloy. *Int J Adv Manuf Technol* 112(11):3399–3413. <https://doi.org/10.1007/s00170-021-06588-4>
- Li ZC, Jiao Y, Deines TW et al (2005) Rotary ultrasonic machining of ceramic matrix composites: feasibility study and designed experiments. *Int J Mach Tools Manuf* 45(12–13):1402–1411. <https://doi.org/10.1016/j.ijmactools.2005.01.034>
- He YH, Wan RQ, Zhou JJ et al (2017) Modeling for surface roughness of hard and brittle materials in axial ultrasonic vibration grinding. *J Vib Shock* 36(23):194–200. <https://doi.org/10.13465/j.cnki.jvs.2017.23.029>
- Cao Y, Yin JF, Ding WF et al (2021) Alumina abrasive wheel wear in ultrasonic vibration-assisted creep-feed grinding of Inconel 718 nickel-based superalloy. *J Mater Process Technol* 297:117241. <https://doi.org/10.1016/j.jmatprotec.2021.117241>
- Lin SY (2002) Study on the prestressed sandwich piezoelectric ceramic ultrasonic transducer of torsional-flexural composite vibrational mode. *J Acoust Soc Am* 112(2):511–517. <https://doi.org/10.1121/1.1492819>
- Gao GF, Xia ZW, Yuan ZJ et al (2021) Influence of longitudinal-torsional ultrasonic-assisted vibration on micro-hole drilling Ti-6Al-4V. *Chin J Aeronaut* 34(9):247–260. <https://doi.org/10.1016/j.cja.2020.06.012>
- Chang BQ, Zhao B, Yuan LS et al (2019) Influence of force load on ultrasonic longitudinal-torsional composite drilling system. *J Vib Meas Diagnosis* 39(05):1111–1119. <https://doi.org/10.16450/j.cnki.issn.1004-6801.2019.05.029>
- Qian XH, Shen MH (2011) A new standing-wave linear moving ultrasonic motor based on two bending modes. *Appl Mech Mater* 101–102:140–143. <https://doi.org/10.4028/www.scientific.net/AMM.101-102.140>
- Yuan LS, Zhao B, Wang Y et al (2020) Surface micro-texture characteristics of 7075 aluminum alloys by elliptical vibration assisted turning. *China Mech Eng* 31(15):1831–1838. <https://doi.org/10.3969/j.issn.1004-132X.2020.15.010>
- Zhao B, Bie WB, Wang XB et al (2019) The effects of thermo-mechanical load on the vibrational characteristics of ultrasonic vibration system. *Ultrasonics* 98:7–14. <https://doi.org/10.1016/j.ultras.2019.05.005>
- Zhao B, Guo XC, Bie WB et al (2020) Thermo-mechanical coupling effect on surface residual stress during ultrasonic vibration-assisted forming grinding gear. *J Manuf Process* 59:19–32. <https://doi.org/10.1016/j.jmapro.2020.09.041>
- Li JJ, Cheng CJ (2005) Differential quadrature method for non-linear vibration of orthotropic plates with finite deformation and transverse shear effect. *J Sound Vib* 281(1–2):295–309. <https://doi.org/10.1016/j.jsv.2004.01.016>
- Qu YG, Long XH, Yuan GQ et al (2013) A unified formulation for vibration analysis of functionally graded shells of revolution with arbitrary boundary conditions. *Compos Part B-Eng* 50:381–402. <https://doi.org/10.1016/j.compositesb.2013.02.028>
- Wang QS, Shi DY, Shi XJ (2016) A modified solution for the free vibration analysis of moderately thick orthotropic rectangular plates with general boundary conditions, internal line supports and resting on elastic foundation. *Meccanica* 51(8):1985–2017. <https://doi.org/10.1007/s11012-015-0345-3>
- Li WL (2004) Vibration analysis of rectangular plates with general elastic boundary supports. *J Vib Shock* 273(3):619–635. [https://doi.org/10.1016/S0022-460X\(03\)00562-5](https://doi.org/10.1016/S0022-460X(03)00562-5)
- Li GR, Wang L, Hu CB et al (2020) Analysis of transverse vibration characteristics for stiffened rectangular plates with classical boundary conditions. *J Vib Shock* 39(16):261–266. <https://doi.org/10.13465/j.cnki.jvs.2020.16.035>
- Du F, Ma TB et al (2017) Study on new method for modal parameters identification of stiffened plate with four clamped edges. *Vib Procedia* 14. <https://doi.org/10.21595/vp.2017.18972>
- Paula Macanhan VB, Correa EO, de Lima AMG et al (2019) Vibration response analysis on stainless steel thin plate weldments. *Int J Adv Manuf Technol* 102(5–8):1779–1786. <https://doi.org/10.1007/s00170-019-03297-x>
- Selicani GV, Buiocchi F (2021) Stepped-plate ultrasonic transducer used as a source of harmonic radiation force optimized by genetic algorithm. *Ultrasonics* 116. <https://doi.org/10.1016/j.ultras.2021.106505>
- Wang RH, Han Q, Li PJ et al (2012) Geometrically nonlinear free vibration and internal resonance of a stiffened plate with four edges simply supported. *J Vib Shock* 31(24):60–64. <https://doi.org/10.13465/j.cnki.jvs.2012.24.001>
- Podymova NB, Karabutov AA (2021) Transformation of laser-induced broadband pulses of longitudinal ultrasonic waves into pulses of shear waves in an isotropic solid plate immersed in a liquid. *Ultrasonics* 116. <https://doi.org/10.1016/j.ultras.2021.106517>
- Heikkola E, Laitinen M (2005) Model-based optimization of ultrasonic transducers. *Ultrason Sonochem* 12(1):53–57. <https://doi.org/10.1016/j.ultsonch.2004.05.009>
- Piao C, Kim JO (2016) Vibration characteristics of a piezoelectric disk laminated with an elastic disk. *J Mech Sci Technol* 30(12):5351–5362. <https://doi.org/10.1007/s12206-016-1102-9>
- Iula A, Vazquez F, Pappalardo M et al (2002) Finite element three-dimensional analysis of the vibrational behaviour of the Langevin-type transducer. *Ultrasonics* 40(1):513–517. [https://doi.org/10.1016/S0041-624X\(02\)00174-9](https://doi.org/10.1016/S0041-624X(02)00174-9)
- Lin S, Xu L, Wen XH (2011) A new type of high power composite ultrasonic transducer. *J Sound Vib* 330(7):1419–1431. <https://doi.org/10.1016/j.jsv.2010.10.009>
- Xu L, Lin S, Hu W (2011) Optimization design of high power ultrasonic circular ring radiator in coupled vibration. *Ultrasonics* 51(7). <https://doi.org/10.1016/j.ultras.2011.03.010>
- Yin S, Zhao B, Li Y (2019) Design of a mode conversion type longitudinal-torsional composite ultrasonic vibration machining system. *J Vib Shock* 38(11):242–248. <https://doi.org/10.13465/j.cnki.jvs.2019.11.035>
- Jun Pi (2008) Longitudinal-torsional vibration converter of cylinder with multiple diagonal slits. *J Mech Eng* 05:242–248. <https://doi.org/10.3321/j.issn:0577-6686.2008.05.041>
- Lin SY, Zhang FC (1992) A study of large dimension vibrating systems and their transverse slotting. *Technical Acoustics* 04:24–28. http://sxjs.cnjournals.cn/ch/reader/view_abstract.aspx?file_no=19920407&flag=1

34. Lin ZM, Lu JH (1996) Analysis of ultrasonic horn for plastic welding by finite element method. *Technical Acoustics* 04: 153–156. http://sxjournals.cn/ch/reader/view_abstract.aspx?file_no=19920407&flag=1
35. Lu X, Hu J, Peng H et al (2017) A new topological structure for the Langevin-type ultrasonic transducer. *Ultrasonics* 75:1–8. <https://doi.org/10.1016/j.ultras.2016.11.008>
36. Gao J, Lin SY (2009) Study on the oblique wedge-like transformer with a large dimension rectangular gradual section. *J Shaanxi Norm Univ (Nat Sci Ed)* 37(05):42–44. <https://doi.org/10.1360/972008-2465>
37. Xu L, Qiu X, Zhou J et al (2018) A 2D dual-mode composite ultrasonic transducer excited by a single piezoceramic stack. *Smart Mater Struct*. <https://doi.org/10.1088/1361-665X/aaf275>
38. Azarhoushang B, Tawakoli T (2011) Development of a novel ultrasonic unit for grinding of ceramic matrix composites. *Int J Adv Manuf Technol* 57(9):945. <https://doi.org/10.1007/s00170-011-3347-x>
39. Han GC, Sun Y, Sun M et al (2014) Design and simulation for a porous rectangular block ultrasonic horn. *J Vib Shock* 33(19):211–217. <https://doi.org/10.13465/j.cnki.jvs.2014.19.036>
40. Zhou GP, Liang MJ, Wang JX (2004) Study on large sized ultrasonic vibrators. *Tech Acoust* 03:183–188. <https://doi.org/10.3969/j.issn.1000-3630.2004.03.012>
41. Xian XJ, Lin SY (2008) Study on the multi-frequency piezoelectric ultrasonic transducer with arectangular radiator. *J Appl Acoust* 03:234–238. <https://doi.org/10.3969/j.issn.1000-310X.2008.03.013>
42. Bruzzone AAG, Costa HL, Lonardo PM et al (2008) Advances in engineered surfaces for functional performance. *CIRP Ann* 57(2):750–769. <https://doi.org/10.1016/j.cirp.2008.09.003>
43. Li J, Xiong D, Dai J et al (2010) Effect of surface laser texture on friction properties of nickel-based composite. *Tribol Int* 43(5–6):1193–1199. <https://doi.org/10.1016/j.triboint.2009.12.044>
44. Xing D, Zhang J, Shen X et al (2013) Tribological properties of ultrasonic vibration assisted milling aluminium alloy surfaces. *Procedia CIRP* 6:539–544. <https://doi.org/10.1016/j.procir.2013.03.008>

Publisher's note Springer Nature remains neutral with regard to jurisdictional claims in published maps and institutional affiliations.